THE PENNSYLVANIA STATE UNIVERSITY
SCHREYER HONORS COLLEGE

DEPARTMENT OF ENGINEERING SCIENCE AND MECHANICS

LOCALIZED TEMPERATURE FIELD MEASUREMENTS IN BRAIN VIA THIN-FILM VERTICALLY INTEGRATED VANADIUM OXIDE THERMISTOR ARRAYS

Myles W. Billard

Spring 2015

A thesis
submitted in partial fulfillment
of the requirements
for a baccalaureate degree
in Engineering Science
with honors in Engineering Science

Reviewed and approved* by the following:

Bruce J. Gluckman
Associate Professor of Engineering Science and Mechanics
Thesis Supervisor

Mark W. Horn
Associate Professor of Engineering Science and Mechanics
Honors Adviser

Judith A. Todd
Department Head
P.B. Breneman Chair and Professor of Engineering Science and Mechanics

* Signatures are on file in the Schreyer Honors College and Engineering Science and Mechanics Office.

Abstract

Temperature plays a significant role in neurological function in normal and pathological brain physiology. Examining how temperature fields change within and between different regions of brain, and on a scale relative to the vasculature and neuronal cells that make up brain tissue, could help better characterize and understand the subtleties of neural activity in various physiological conditions such as wake and sleep, and in pathologies such as epilepsy. A device that is capable of localized, chronic temperature field recordings must be sensitive, must not disrupt surrounding tissue with its mechanics or size, must be biocompatible, and must not influence tissue with local heat dissipation or thermal shunting.

A novel vertically-integrated vanadium oxide (VO_x) thermistor array deposited on flexible polyimide substrate has been developed for measuring local temperature field dynamics in capillary and neuronal networks for rats with a Tetnus Toxin model of epilepsy [1]. Acquisition electronics were developed to interface an array of eight thermistors to Dr. Gluckman's PSU EEG-8 biopotential recording system. Samples of VO_x deposits on glass and polyimide substrates with an active temperature sensing area of 10 µm × 10 µm were tested *in-vitro* for thermal characteristics and ability of parylene-C passivated samples to record in saline solution. Results from two samples showed temperature coefficient of resistance (TCR) values of -4.04 %/℃ and -4.53 %/℃ with nominal resistances for functioning thermistors of about 1.3 MΩ. Analysis of a working channel used in the bulk-heat temperature experimentation showed a real-time average TCR of -4.4 %/℃ over a 5 ℃ temperature change. Passivated polyimide samples were able to record for an hour in liquid ionic solution. Additionally, a method for surgical implantation of our device has been developed using polyethylene glycol (PEG) encapsulation and 25 µm thick (1 1 1) type silicon shuttles for insertion assistance. 20 µm thick polyimide

strips taken from deposition samples were inserted into 0.6% agarose gel to simulate brain implantation. Additional *in-vitro* experiments must be performed to test the array's ability to measure small, controlled temperature gradients. Future *in-vivo* experiments will be conducted to monitor real-time, localized temperature field dynamics in brain.

Table of Contents

List of Figures

Acknowledgments

This thesis project is the culmination of my time and efforts as an undergraduate at Penn State. It has taken me to the highs of pursuing my scientific passions and to the lows of little sleep and a lot of stress. Over the course of these past several years, many people have provided me with their help, guidance, support, or criticism when I needed it most. Without these people, I would not have been able to accomplish the things that I am most proud of during my time here, this thesis being one of them.

I would first and foremost like to thank my thesis advisor, Dr. Bruce Gluckman. Dr. Gluckman took me into his lab at the Center for Neural Engineering my Sophomore year and introduced me to the field of research that I now know and love. He has supported me emotionally and academically, and has had a profound impact on the person I envision myself to be in the years to come. I am very happy to be continuing my Master's research with him over the next year.

Next, I would like to thank the list of people who helped make this thesis happen, in no particular order. As my faculty reader and a collaborator on this project, Dr. Mark Horn has helped me with a lot of technical issues and has provided guidance for this project. Dr. Hitesh Basantani, another key collaborator, worked many hours to fabricate the devices used in this project, and helped me through much of the testing and understanding that went into this thesis. Dr. Jackson and his lab members provided me with access to essential testing equipment that I needed to characterize my devices. Dr. Gary Gray and Dr. Francesco Costanzo went out of their way to help me with many technical issues that I had with LaTex. All these people were essential to the completion of this thesis.

I would also like to thank members of Dr. Gluckman's lab, who I have had the privilege of getting to know and work alongside during my time at Penn State. Balaji Shanmugasundaram, Anjum Parkar, Madineh Sarvestani, Andrew Alexander, and Fatemeh Bahari were all there for me when I was stressed, confused, or simply needed someone to talk to during the long hours that went into this project.

I would like to acknowledge the Penn State College of Engineering for supporting part of my research through funding from a Summer Research Initiative grant.

And lastly, I would like to thank my family and all my friends, who have unconditionally supported my goals and were there for me during my greatest successes and hardest failures. Without them, none of this could have happened.

Chapter 1

Thesis Synopsis

The project to be presented in the following pages was a collaborative effort between groups at Penn State with multidisciplinary backgrounds aimed at designing a neural implant to study localized temperature fields in brain. Temperature has a significant influence on neurological function in both normal and abnormal brain, and deviations from brain's homoeothermy can be linked to changes in behavioral states, neuronal cell activity, and neural pathologies. Our collective team of researchers includes Dr. Gluckman from the Center for Neural Engineering, Dr. Horn and Dr. Basantani from the department of Engineering Science and Mechanics, and myself, with the help of Dr. Jackson and his students from the thin-films group at Penn State. We have developed a minimally-invasive, highly localized vanadium oxide thermistor array capable of measuring small temperature gradients in brain on a thermal and spatial scale that surpasses most contemporary neural temperature sensing devices.

The device and its development truly reflects the multidisciplinary nature of neural engineering. For this project, people from different engineering and science backgrounds have come together, combining very specialized frames of knowledge, in an effort to create something well beyond the sum of its individual parts. The

creation and fabrication of the novel through-film thermistor design was the work of Dr. Horn and Dr. Basantani. The vision to transform what was originally a device purposed for infrared imaging into a viable biomedical tool was Dr. Gluckman's. My role was to assess the feasability of that vision, given the performance capabilities of the design, and engineer the thermistor into an implantable array that can be used for chronic temperature recordings. I helped guide the elements of the array's design with an understanding of brain physiology, and used electronics and experiments I designed, with oversight from Dr. Gluckman, to characterize our neural implant and turn it into a fully functioning temperature measurement system.

The narrative of this thesis begins with an examination of brain temperature and how small changes in temperature fields within and between different brain regions play a role in affecting neurological functions. This chapter also includes the background to the main motivation for my efforts on this project: to design a device that uses key biopotential measurements to better understand certain brain pathologies, specifically epilepsy, and find a way to use the knowledge gained from that data to improve the lives of people afflicted by those conditions. The thesis then moves into a discussion of measuring temperature, and examining the physics of different temperature sensors, in an extremely sensitive biological system like brain. From this point, the thin-film vanadium oxide thermistor array is introduced. The elements of the implant design, from its physical layout to the acquisition electronics used to record temperature measurements from it, are an application of all the concepts and considerations outlined in the previous chapters. Each piece of the design is presented in a way that helps tie it back to the fundamentals of fabricating an effective biomedical implant for temperature sensing. Afterwards, the rest of the narrative is an overview, analysis, and discussion of the experiments used to characterize the array, the methods developed to turn it into a viable neural

implant, and the results of these efforts.

Chapter 2

Temperature in Brain

Temperature has tremendous physiological importance in brain, playing a key role in neural activity and function. In normal physiology, local and widespread neural temperature changes can be observed between various behavioral states, such as wake and sleep, and between states with different intensities of mental activity, such as relaxation versus performing numerical calculations. In pathological brain, hyperthermic temperature fluctuations can cause seizures and permanent cell damage. For specific afflictions like epilepsy, sudden temperature change can be a characteristic indicator of oncoming symptom expressions. Also, temperature gradients are present within and between brain's different topographical regions. The various inter-cranial thermal relationships that make up neural homoeothermy are still not well understood, as measuring small temperature fields deep within brain is difficult. Examining how temperature changes based on neurological and physiological states, and how those fluctuations can influence local and global neurological function, is a fundamental goal of neuroscience. Revelations from these sorts of studies could lead to great advances in how we understand brain and how we treat patients with abnormal neural function. This chapter takes a look at the biology of brain temperature, in normal and pathological brain, and seeks to

explain why studying temperature and its relationship to brain is so interesting and important.

2.1 Brain Temperature in Normal Physiology

Brain exists in a dynamic thermal homoeostasis, or homoeothermy. This homoeothermy, influenced by factors such as cell metabolism, external environments, and arterial blood flow, typically fluctuates within the small and distinct range of 34 ℃ to 39 ℃ [2]. This temperature range, which is an overall average for brain, is higher than both body-core and arterial blood [3] [4]. This is partially because, despite only accounting for two percent of overall body mass, brain consumes approximately twenty percent of the body's total oxygen intake and oxygen requires heat to be chemically released from hemoglobin [5] [6] [7]. Additionally, while regular cells absorb power on the order of pico-Watts, neurons require a few nano-Watts to fully function [8]. All of that energy ends up being dissipated as heat after metabolic processing. This suggests brain requires a large amount of heat generation to maintain cell activity [6].

In normal physiological conditions, temperature in brain is constantly changing. The relationship between neural activity and heat dissipation creates complex thermal patterns throughout brain. These patterns are affected by things such as behavioral state, physical activity, and the environment. Temperature can vary from wake to sleep, and from conditions of stress to relaxation. Brain's homoeothermy is so dynamic that there are even temperature differences from region to region, both locally and generally. Temperature can have a significant influence on neural function by changing spike amplitudes and signal conductance in neurons. Given all of these factors, it is clear that understanding physiologically normal brain

temperature is no simple task. It is, however, an essential part of understanding why brain temperature is such an interesting scientific problem.

2.1.1 Temperature in Relation to Behavioral States

Brain is in a continual state of function, no matter what one is doing. Neuron spike rates and firing amplitudes, as well as blood flow and cell metabolism, increase and decrease with different behavioral states, and consequently so do brain temperatures. Wake and sleep are the two fundamental behavioral states that animals undergo on a daily basis. Within each though there are various subtleties, like arousal levels and sleep phases, that distinguish local and widespread neural activity and have characteristic temperature changes associated with them. This section reviews temperature and its relation to these different behavioral states.

2.1.1.1 Wake

Humans, like most animals, are awake for the majority of the day. The wake behavioral state can be characterized by high amplitude and de-synchronous cortical activity, with spectral frequencies varying in different areas of brain. While awake, we engage in constant information processing. Sensory input and stresses from the surrounding environment cause neurons to fire. So do the performing of mental tasks, like numerical calculations. Increased neural activity is thought to be associated with increased metabolic processing and localized heat dissipation. This suggests that many things humans do throughout the day, within the wake behavioral state, could have correlated temperature increases in areas of brain that are being used to process relevant information and actively think.

In a study done by Yablonskiy et al. [9], very small localized temperature

fluctuations, approximately 0.01–0.2 ℃, were detected in volunteers laying down in a fMRI machine who underwent visual stimulation via LED lights. The temperature changes appeared in the visual cortex, whereas the rest of brain did not change much above or below average temperatures. Blood flow was also shown to have increased to the visual cortex during stimulation, further promoting the idea that blood flow is inherently linked to localized temperature field changes. In 2002 Kiyatkin et al. [10] measured brain temperatures in three separate brain regions (dorsal and ventral striatum, and cerebellum) in rats. The temperatures in each brain region changed, with respective differences, to different environmental stimuli, like cage transfers and sexual arousal. The study was done using thermocouples with 125 µm wires and 400 µm tips. Temperature changes were recorded throughout various challenges. For example, a tail pinch increased base temperatures in each monitored region after different respective lengths of time. Similar results occurred with the other challenges. The group's overall conclusion was that, because brain temperature was above arterial blood temperature and increased with greater magnitude, the metabolic processes associated with neural activity are the primary cause of brain temperature changes. Lastly, though not the first one to do so, Dittmar et al. showed in 2006 brain temperature elevations of several tenths of a degree Celsius while subjects performed mental math using a non-invasive temperature sensor. This implicates that increased intensity of thought is associated with higher regional temperatures [11]. While this is not a comprehensive list of contemporary literature on the subject, it is reflective of the conclusions reached by many other studies relating various stimuli and neural activity to brain temperature, as reviewed, for example, by Rango [2] and Kiyatkin [3].

2.1.1.2 Sleep

Sleep seems to be a critical part of brain's memory and recovery [12]. Regular sleep (synchronized sleep) occurs in phases of non-rapid and rapid eye movement, or NREM and REM, respectively. Still more specific, within REM sleep there are tonic and phasic phases. Tonic REM is characterized by generalized, low-amplitude theta rhythms throughout the hippocampus. Theta rhythms are synchronous neural signals with a frequency range of 5–12 Hz [13]. Tonic REM also decreases neck and facial muscle movement and has a signature tenths of a degree C widespread brain temperature increase associated with it [14] [15]. During phasic REM, specific oculomotor movements and other distinct body activity occur, as well as high 8–12 Hz alpha band spectral power density relative to other bands [14].

Parmeggiani suggests that the mechanisms of temperature rise during REM may be related to metabolic activity in nerve tissue, changes in arterial blood flow and temperature, and a decrease in selective preoptic-hypothalamic brain cooling activity [15]. Clearly, transitions from one REM phase to another, and from NREM and REM cycles, are characterized by many different but distinct physiological changes in brain, with temperature being a main one. Monitoring localized temperature gradients during sleep activity could be an effective way of immediately knowing what phase of sleep an animal is in, as well as provide an understanding of how different physiological factors, like cellular activity, blood flow, and hypothalamic temperature regulation, change and affect local areas of brain during sleep behavior.

2.1.2 Effects of Temperature on Neural Function

One final point to discuss when considering brain temperature in normal physiology are the direct effects it can have on neural function. It has been shown that neuronal activity and cell metabolism are fundamentally tied to localized heat generation, but what about the converse: does temperature play a role in changing neuron behavior? The short answer is yes. Brain temperature field fluctuations are intimately tied to the functions of neurons. Schiff and Somjen published a paper in 1985 reporting "The effects of temperature on synaptic transmissions in hippocampal tissue slices" [16]. The experiments were done using 350 µm slices of CA1 rat hippocampus that were stimulated with 50 µA of current using microelectrodes at temperatures of 29 ℃, 33 ℃, and 37 ℃. The results showed a higher membrane potential in the post synaptic connections among the stimulated neuron populations but a decrease in the spike amplitude. This leads to the conclusion that temperature has an effect on a neuron's ability to propagate signals, and possibly on both inter-synaptic conductance and post synaptic excitation thresholds as well. This is only one of several experiments to have shown a correlation between changes in synaptic activity and temperature, as pointed out by Andersen and Moser in a 1995 review paper [17].

2.2 Brain Temperature in Pathological and Injured Brain

Studying brain in a normal, healthy physiology is important and exciting, but another major pursuit of neuroscience is to understand brain that has been afflicted with pathology. Diseases, genetic factors, and everyday accidents can lead to brain

damage, dysfunction, and/or neuronal cell degradation. Because brain is the control center of the body, any abnormalities with its cells can have drastic consequences on its ability to work. Afflictions like epilepsy and Parkinson's disease interfere with normal neural functions, creating problems such as lack of motor control and seizures. A traumatic event like a stroke or head injury can incapacitate entire areas of the brain permanently, causing issues like paralysis, speech impairment, and death. Studying how certain brain parameters, like temperature, change on a local cell and capillary level, in real time, from these pathologies would help scientists better characterize their abnormalities and make progress toward potential therapies, leading to an overall better quality of life for those who have been affected by them.

One way to characterize the effects specific pathologies have on brain is to measure how the temperature fields are changing in damaged areas. Temperature has a significant effect on neural function, even in homoeothermy, so it might stand to reason that it could have an equal, if not greater, impact on brain with severe abnormalities. Neurons are extremely sensitive and can become damaged in temperatures lower and higher than that of their typical physiological range, sometimes with irreversible effects [18] [19]. Also, as discussed earlier, temperature can have an influence on synaptic transmissions. Thus, a hypothesis could be made that temperature might change in some significant way during an extreme physiological event like a seizure or stroke. Indeed, there have been studies to support such claims. Furthermore, if temperature plays such a critical role in certain brain pathologies, it may be valid to suggest that forcing an artificial temperature change, i.e. localized heating or cooling, might mitigate or even eliminate the severity of pathological events. Ultimately, it is paramount to understand how local and global temperature fields influence the symptoms, severity, and progression of

various pathological conditions.

2.2.1 Temperature Fluctuations in Seizure Activity

2.2.1.1 Epilepsy

Epilepsy is a neurological disorder that affects over 2 million people in the United States, or roughly one percent of the population. This number is estimated to increase to approximately ten percent in populations of developing countries, the majority of those people being children. Epilepsy is a disorder characterized by spontaneous, recurrent seizures that are caused by synchronized rapid firing of neurons. Epileptic seizures can be caused by many different things, such as strokes, infections, genetics, and head trauma. The seizures can affect victims in various ways, causing problems like loss of motor function and emotional control, disassociation with reality, and, in severe enough cases, death [20]. Besides being physically debilitating, epileptic patients can experience difficulties in their social lives as well. A seizure can be shocking for those watching and embarrassing for the victim. Additionally, a seizure can cause uncharacteristic mental and emotional behavior in a person who is seemingly cognizant during the event, creating potentially confusing and harmful social interactions. There are anti-epileptic drugs and surgical treatments for epilepsy, but for a good portion of patients these therapies fail to work.

There are many different types of seizures associated with epilepsy, but the two main categories are focal and generalized seizures. As the name suggests, focal seizures affect a localized area of the brain. On the other hand, generalized seizures cause widespread neuronal disruption throughout the brain. Both types of seizures have subtypes that more specifically describe the events. For example,

focal seizures can be simple or complex. The former can affect a person's sensory perception and emotions, while the latter can result in a loss of consciousness. During generalized events, a victim may experience tonic, absence, myoclonic, or other types of seizures, each with their own unique symptoms. Focal seizures can also become generalized seizures [20]. All of these factors, along with the numerous things that can lead to epilepsy, create a disorder that is unique to each individual and that is very complex in its characteristics. While categorizing the various types of seizures is good for describing the general symptoms of a patient's epilepsy, they are merely behavioral or physical observations. It would be very valuable to be able to understand what is going on during a seizure on a cellular level, using highly localized sensors to monitor physiological changes as they happen in real time.

Epilepsy is typically monitored and characterized using an electroencephalogram (EEG) or brain scanning techniques, like CT and MRI. The rapid spikes associated with seizures are easily distinguished from normal brain activity when measuring variations in electric fields. But as mentioned previously, neuronal activity is inherently linked to temperature field changes. Thus, an additional way to study epilepsy would be to measure temperature fluctuations, both localized and generalized, during seizure events. In fact, neuroscientists have been doing that for many years. Dymond and Crandall showed in 1973 [21] significant temperature changes of approximately a 1–1.5 K near seizure foci within anterior hippocampal gyri roughly half a minute prior to an oncoming seizure event. They attributed the temperature changes to increased neural activity, cerebral blood flow and higher levels of oxygen consumption used for cell metabolism. In the Dymond and Crandall study, temperature had a slight increase prior to the seizure and then a marked drop upon onset of the event. The cooling during the seizure is most likely attributed to human brain being at a higher baseline temperature than

that of body-core; being at a lower temperature, incoming arterial blood causes a cooling effect in areas with increased flow volume [21] [22] [9] [23]. In rats it is the opposite, and seizures produce a localized temperature increase, as shown by Yang et al. in 2002 [19]. In the study, the rats were anesthetized and recurrent seizures were induced using injections of 4-aminopyridine. Thermocouples measured peak temperature increases of 0.3 ℃ near the surface of the cortex.

2.2.1.2 Febrile Seizures

Another common type of seizure, and one with great clinical importance, is a febrile seizure. Febrile seizures are caused by severe fevers, where high temperatures in brain damage neuronal cells and inhibit normal brain activity [18] [23] [24]. These seizures are commonplace in infants and children, and are estimated to affect 3–5% of that demographic [25]. They are also seen often in patients with severe head trauma [26]. The consequences of frequent and/or prolonged hyperthermia in brain are profound. Detecting the onset of a febrile seizure or even just localized hyperthermia before it occurs could mean the difference between life and death for a patient. Further still, simply having a more accurate picture of how temperature fields are changing in a feverish state and how those changes are affecting surrounding neuronal cells would help scientists better understand this pathology and move closer toward potential therapies.

2.2.1.3 Conclusion

Temperature plays a significant role in seizure activity. It has been shown that seizures can be predicted via small temperature changes more than half a minute prior to the onset of an event. With more sensitive and accurate temperature sensors, it may be possible to detect an oncoming, spatially localized seizure even

sooner. This could prove extremely helpful to the safety and quality of life for those who suffer from epilepsy. There are even possibilities to create feedback mechanisms to induce local hyper- or hypothermia in attempts to reduce seizure intensity. More on the potential applications of this will be discussed in later chapters.

2.2.2 Brain Temperature and Neuronal Injury

Neuronal injury can be caused by many different things. Car crashes, sports accidents, strokes, etc. can all cause permanent damage to brain. The extent of injury due to head trauma and other pathologies, however, can be difficult to assess. Localized hyperthermia is known to occur in humans after head trauma, strokes, and cerebral ischemia [23] [26] [27] [28] [29]. Busto et al. [29] demonstrated that the extent of neuronal damage can be correlated to slight temperature changes in brain after ischemic injury. In the study, temperature gradients within CA1 hippocampus were measured in rats with induced ischemia. The CA1 regions were held at various temperatures during the ischemic event. Damage to local neurons was assessed using histological techniques, revealing more neuronal damage in the hippocampal slices that were kept at higher temperatures. Additionally, rats whose brain temperatures were reduced to mild hypothermic levels (30–31 ℃) showed significantly less neuronal damage upon analysis. This has profound implications for both characterizing neuronal injury using temperature measurements and potentially reducing injury using local and global brain cooling during a pathological episode.

2.3 Summary

Temperature, both in and out of homoeostasis, can reveal a lot about underlying brain mechanics. Developing an invasive sensor to help neuroscientists study

localized temperature fields would help tremendously in moving our understanding of brain forward. The challenge is simply in following the principles for developing invasive biomedical implants for localized brain measurements and then focusing in on the right design. With this in mind, the next chapter will introduce various types of temperature sensors and lay out important considerations in creating an invasive sensor for measuring localized temperature fields in brain.

Chapter 3

Design Criteria for a Localized Brain Temperature Sensor

Brain is the most complex organ which animals possess. Human brain, in particular, is comprised of billions of neurons and even more glial cells [30]. While scientists have been studying brain for centuries, measuring electrical activity, temperature, blood flow, and other physiological markers, there is still much to be learned about the intricacies of its various states and functions. Brain's great physiological complexity results in a system that is defined and affected by many different parameters, most of which vary by location and constantly fluctuate in magnitude. This presents a challenge for characterizing brain and its functions as accurately as possible. It also provides difficulties for neural engineers who aim to develop sensors that can detect very small and highly localized physiological changes in brain.

With a particular interest in brain temperature, this chapter outlines the design criteria and engineering considerations needed for developing a localized brain temperature sensor capable of high spatial and thermal resolution measurements. The device can either be invasive or non-invasive, and the type of temperature

sensor can be either contact or non-contact. Multiple examples of each will be presented from contemporary research literature. In the case of an invasive device, factors that can affect the health of the subject and integrity of the measurements, such as its size, mechanical properties, and biocompatibility, must be addressed for both acute and chronic implantations. For non-invasive devices, accuracy and resolution is often less than their invasive counterparts, so they might not be able to measure very small, localized temperature dynamics. Further still, the physics of how temperature changes are detected by type of sensor dictates what material is used and how sensitive, accurate, and fast their measurements are. Overall, every element that goes into the design of a localized brain temperature sensor must be a direct reflection of the goals that the device aims to accomplish in order to develop the most effective device possible.

3.1 Engineering an Effective Biomedical Implant

Given the engineering objective of developing a localized invasive sensor for brain, a good place to start would be to consider what characteristics might make up an effective implantable device. Size, shape, mechanical properties, measurement accuracy, and temporal response are all important in the definition of a sensor. Even more important, however, are how those attributes interact with brain matter and its surrounding environment. A good sensor must record quick and subtle changes in very small areas of brain without creating excessive interference or damage to the activity and tissue around it. It must also maintain recording stability and sensitivity as well as structural integrity within the harsh ionic cerebral spinal fluid (CSF) in which brain sits. Additionally, it must be made with materials that do not invoke a major immune response and compromise device or tissue health in both

the short and long-term. In other words, the parts of the device that are exposed to brain and CSF must be biocompatible. All of these things have to be taken into account when designing a localized invasive sensor for brain.

3.1.1 Mechanical Characteristics

With the general criteria for a good implantable device having been outlined, it is now necessary to fill in the details of each element with a specific understanding of brain physiology. Concerning the mechanical aspect of the design, brain tissue is very soft. The moduli of elasticity in different regions range from 0.5 Kpa to 3 Kpa [31] [32], though this can change dramatically in the presence of chronic implants [32]. Thus, the stiffness of the device cannot be exceedingly high or the mechanical mismatch will strain and scar the surrounding tissue during both insertion and recording [33] [34]. This could greatly reduce the integrity of measurement signals, as scarred neuronal cells have a much higher electrical impedance than living tissue [33]. Brain is also living; it moves and pulsates with micromotions caused by heart beats and changes in blood flow [32]. An invasive sensor should be flexible and compliant to the micromotions of the local tissue surrounding it, as to not cause excessive damage and biological disruption. A competing challenge is that if the device is too flexible it might have trouble being inserted into brain tissue during surgical implantation. This point is discussed in greater detail in later chapters.

Most of these considerations can be successfully addressed with careful choosing of the device materials. Though size too plays an important role, as implants must displace tissue in order to record neural activity [35]. For sensors that are deposited onto a substrate, because of its size relative to the sensor, the overall mechanical properties of the device tend to be dominated by the substrate material. Polymers,

typically 15–35 µm in thickness, with moduli of elasticity on the order of a few GPa are often used as flexible substrates for neural implants. Common materials include polyimide, parylene, and polytetrafluoroethylene (PTFE) [36] [37] [38] [39] [40] [41]. Sensors that cannot be made from more mechanically compliant materials, like metal thermocouples, are not ideal for chronic implantation [33], but are still fairly suitable for acute recordings. All in all, the mechanical properties of an invasive device and their impact on local tissue play a critical role in affecting integrity of recordings and long-term damage done to brain.

3.1.2 Relative Size

The vascular network that pervades brain tissue is intricate and vast. Delicate capillaries exist in dense beds of hundreds of branch profiles per square millimeter [42]. These capillaries are the primary vehicles for delivery of oxygen to brain. And since oxygen is a key factor in cell metabolism, capillaries play a significant role in brain temperature regulation. Their diameters are small though, on the order of 5–7 microns. Thus, the distance between any two microvessels can be tens of microns in length [43]. A highly localized sensor should fit into that intercapillary distance, recording possible differences in parameters like oxygen delivery rate or temperature between two individual microvessels.

Additionally, the size of neurons should be taken into account. This includes diameters of soma, which are the central cell bodies, and axons, which are the branches where action potential propagate. A soma can range anywhere from several microns to tens of microns in width. This means that a good sensor should have an active recording area somewhere in between that range. The axons, however, have narrow diameters, on the order of 2–20 µm, but can have axial lengths varying from

a few microns to tens of centimeters [30]. This can create difficulties in getting high spatial resolution or a complete picture of the changing parameter being measured during recordings. For this reason, invasive sensors must specifically cater their physical dimensions to the objects from which they intend to record.

3.1.3 Biocompatibility

The last major consideration for any neural implant is biocompatibility. Whether the device is intended to be used for acute or chronic recordings, it is important that no component is cytotoxic and that its presence creates as little an immune response as possible. Besides consideration for the host's health, this is also because fibrous encapsulation from a foreign body response and scarring or death of local neuronal cells will decrease the electrical performance of sensors measuring local biopotentials in brain [33] [41] [44]. Unlike the early days of biomedical implants, when a good material was one that did not poison the host or create irreversible tissue damage [45], today's technology offers a wide variety of relatively inert materials, such as polyimide, parylene, and silicon, that can be used as substrates and protective coatings to make devices more biocompatible. It is also important to make sure that the materials used as substrates or for passivation do not interfere with necessary electrical or mechanical activity of the sensor.

Biocompatibility of a material can be assessed in a variety of ways. In 1993 Richardson Jr. et al. tested several materials for biocompatible performance using protein adsorption, cell culture cytotoxicity, platelet clotting times, and surface characterization [36]. A more in depth look at Richardson Jr.'s experiments and analysis can be found in the "Array Substrate" section of chapter 4 where the biocompatibility of glass and polyimide is discussed. An important takeaway from

the study though is that biocompatibility is not a simple binary matter. All materials, even ones labelled as biomaterials, sit on a spectrum of biocompatibility, where some perform better or worse than others depending on what is being evaluated. No non-native biological material, however, is truly biocompatible.

Another study demonstrating an assessment of biocompatibility, done by Lago et al. in 2007, used two longitudinal intrafascicular gold electrodes (LIFE), one made of a platinum core and the other of polyimide [41]. Tests included observing electrophysiological and morphological/ immunochemical changes in surrounding sciatic nerves and tissue after 30, 60, and 90 days of electrode implantation using non-invasive nerve stimulation tests and post-implant histological evaluations. Nerve latency and fibrous encapsulation were observed from both electrodes, but the results were less severe in the case of polyimide. Another important observation from this study was the presence of corrosion and delamination on the Pt electrode over the time course of implantation. Platinum, like many other metals used for biopotential recordings, is toxic to the body, and any amount of corrosion can be harmful. For this reason, passivation of neural implants with polymers like polyimide or parylene to protect devices from corrosion in brain's harsh ionic environment is now a common practice.

In summary, biocompatibility of component materials is one of the most important aspects to consider when designing a biomedical implant, especially one purposed for chronic recordings. This is both for biological health and sensor performance reasons. Immune responses to local cell damage and death can be detrimental to the overall integrity of measurement signals and would most likely not be representative of activity measured from living, healthy brain tissue. There are many materials readily available that can be used to improve the biocompatibility of an invasive device, and techniques like implant passivation are essential to

protecting both the brain and neural implant.

3.2 Temperature Sensors

Here I present a discussion of various sensors used for brain temperature measurements. This section begins with an overview of the types of sensors, both invasive and non-invasive, available to neural engineers and provides examples of their use in the field. Each device has advantages and disadvantages relative to one another, and all aspects of the devices must be taken into account. As discussed earlier, a good sensor must be sensitive, accurate, and if possible, biocompatible and minimally invasive. It must also resolve measurements on a thermal, temporal, and spatial scale specific to the task at hand. Ultimately, there is much to consider before moving forward in selecting the best type of sensor for the design of a new device. This section, along with the earlier topics in this chapter, will lead directly into the introduction of our novel vanadium oxide thermistor array neural probe presented in the following chapter.

3.2.1 Contact Temperature Sensors

The majority of temperature sensors used in neuro-scientific research are contact type. These sensors can be invasive or non-invasive, but they must be in physical contact with the mensurand from which they are detecting temperature. Thermocouples, thermistors, resistance temperature detectors (RTDs), and specially designed transistors are all examples of contact temperature sensors. There are, however, important differences between each device that must be taken into account when designing a highly localized and sensitive temperature measurement system in brain. How temperature change is detected, the physical requirements for the

sensor, and how well it can be implemented as a chronic implant all affect its utility as a quality neural engineering tool. The following sections will help describe each device in detail, as well as provide examples of their use in neuroscience, so that the key differences between them can become apparent.

3.2.1.1 Thermocouples

A thermocouple is a device that uses a physical phenomenon called the *Seebeck effect* to measure temperature change. The Seebeck effect is created from the junction of two dissimilar metals. This junction generates a small voltage and does not need external excitation to operate, thus making it a passive transducer. This voltage, called the *Seebeck voltage*, is temperature dependent and is described by the following equation:

$$V = -S(T_C - T_H) \tag{3.1}$$

S is the Seebeck coefficient. Typical values for S are around 50 µV/℃ [46].

T_H is the higher junction metal temperature

T_C is the junction metal temperature

Thermocouples have several advantages over other contact sensors. They can be used in a very wide range of temperatures, between negative hundreds to thousands of degrees Celsius. They also generally have fast time constants, around 0.1-10 s, so they are generally good for real-time measurements. Another advantage is that they are rugged and can resist possible electrical or physical damage [46] [47]. Lastly, thermocouples are cheap and their complementary circuitry is relatively easy to design. For these reasons, thermocouples have been and still are commonly employed for brain temperature research.

There are, however, some major disadvantages to using a thermocouple as a localized invasive temperature sensor. First off, the accuracy of thermocouples is low, around 0.5–5 ℃ [47] [46]. This would not be ideal for measuring minute changes in temperature fields around capillary beds and neuronal cells. Additionally, they are not as sensitive as some other sensor types. Their long metal leads are also an issue, as they are much stiffer than brain tissue and can act as conduction sources in thermal gradients. As discussed in the "Mechanical Characteristics" section of this chapter, the mechanical mismatch, which is many orders of magnitude in modulus of elasticity, can potentially create significant damage to brain. A thermocouple probe is also likely to have a higher thermal conduction than that of brain tissue, causing a thermal shunting effect would create inaccuracies in spatially resolved temperature measurements [48]. A final disadvantage of thermocouples is the need for a reference junction. This reference junction would be from another, same type thermocouple that is held at a fixed temperature, typically in an ice bath at 0 ℃. The more accurate the measurements need to be, the more stable the reference junction must be [46].

Many previously cited studies have used thermocouples as a means of measuring brain temperature [4] [10] [19] [28]. A more recent study performed by Lee et al. [49] used a microfabricated thermocouple array to measure temperature within and outside of mouse thalamus. The device consisted of a four T type thermocouples deposited on a silicon probe. Each junction was 400 μm^2. Altogether, the average S was 15.12 µV/℃ and the time constant was 0.78 s. The paper did not specify how accurate their measurements were. The measured internal-external thalamus temperature difference was reported as 4 ℃.

3.2.1.2 Resistance Temperature Detectors

A resistance temperature detector is a coiled wire or film made of a pure metal or alloy whose resistance changes linearly with temperature, as shown by the equation:

$$R_T = R_0[1 + \alpha(T - T_0)] \tag{3.2}$$

R_T is the resistance at temperature T

R_0 is the resistance at room temperature

α is the temperature coefficient of resistance of the metal (1/℃)

RTDs are commonly made of either copper or platinum and can operate in a wide range of temperatures, -260 ℃ to 650 ℃. They are very stable over a long period of time with drifting less than 0.1 ℃/year [50]. They are also quite accurate with temperature variations as low as several m℃. Furthermore, they have positive temperature coefficients (PTC), which is a parameter representing device sensitivity, of around 400 mV/℃. Some drawbacks of RTDs are: they are active devices, so they require current excitation to work; they are expensive; and they have a slower response time than other contact temperature sensors [47].

A recent study of brain temperature using RTDs was done in 2011 by Li et al. [51]. The group developed a smart catheter temperature sensor using a thin-film gold RTD. The active sensor area was very large, 775 µm × 900 µm, with a resistance of about 100 Ω and a sensitivity of 67.95 mV/℃. The temporal response of the device was 950 ms while the accuracy was 0.1 ℃. RTDs are not employed too often in neural probes, but they could be well suited for invasive local temperature measurements due to their stability and accuracy. The size of the device , however, would have to be significantly reduced.

3.2.1.3 Thermistors

Thermistors are active semiconductor devices typically made from ceramics or metal-oxides that measure temperature change based on characteristic changes in their material's resistance. The temperature dependence of resistance is non-linear and follows an Arrhenius relationship for thermal activation:

$$R_T = R_0 e^{-E_a/k_B T^2} \tag{3.3}$$

R_T is the thermistor resistance at temperature T

R_0 is the thermistor resistance at room temperature

k_B is Boltzmann's constant

E_a is the activation energy of the thermistor material

The exponent in equation 2.3 is called the temperature coefficient of resistance (TCR) of the material and is described in units of %/K by the following equation:

$$TCR = -E_a/(k_B T^2) * 100 \tag{3.4}$$

A thermistor can have either a positive or negative TCR (PTC and NTC, respectively). Most thermistors, however, are of the NTC type. This means that their resistance decreases as temperature increases. One must be careful when working with this effect, however, as the reduced resistance in increased temperature environments can create a runaway effect from the self-heating caused by current excitation. If the Joule heat, as it is known, is not effectively dissipated, an overdraw of current and overheating may occur, causing measurement inaccuracies and possibly destroying the device [52]. Most NTCs for thermistors are between -2 %/℃ and -6 %/℃ and typical R_0 values are on the order of a few kΩ [46] [47].

The standard operating range of thermistor devices is smaller than that of a thermocouple and RTD, but is still well beyond the limits of any biological system from which temperature would be measured.

The major disadvantage of a thermistor is that the TCR can drift if the active semiconductor material is not passivated well from external environments. This may create a loss of sensitivity over time. Thermistors have the advantage though of being very accurate with small time constants. This makes them attractive for real-time localized brain temperature measurements. Additionally, they are some of the most sensitive contact devices available, making them ideal for small measurements over a narrow temperature range [52]. Lastly, they have a low cost and can be nano-fabricated into many shapes and onto many substrate materials. This includes flexible polymers that will potentially do less damage to brain. These features allow for the design of a minimally invasive neural probe to be greatly simplified.

Thermistors are a commonly used device in brain temperature research, as they are small, sensitive, and accurate. Many of the studies referenced in the introduction and background used thermistors, including Dymond et al. [21] [22], Rossi et al. [23], and Rumana et al. [26], among others [27] [29]. As fabrication techniques continue to improve and smaller, more sensitive thermistor materials are discovered [53] [54] [55], thermistors are quickly becoming one of the most attractive devices for invasive neural temperature probes. In the invasive sensor branch of neural engineering, the aim is to develop minimally invasive, highly accurate, and highly sensitive devices. This thesis itself aims to introduce one of the most advanced iterations of implantable thermistor technology available in neural research.

3.2.1.4 Integrated Circuit Thermometers

The final type of contact sensor relevant to the discussion of contact temperature sensors are integrated circuit (IC) thermometer. These devices use thermally-dependent electrical characteristics of diodes or transistors to sense temperature changes. It is well known that current flow through a diode follows the famous Shockley equation:

$$I = I_s(e^{V_D/nV_T} - 1) \tag{3.5}$$

I is the current flowing through the diode

I_s is the saturation current at room temperature

V_D is the voltage across the diode

I_s is reverse bias saturation current

V_T is the thermal voltage

V_T is the temperature-dependent factor by which a diode, bipolar junction, or MOSFET can become a viable thermometer, as seen in the following equation:

$$V_T = \frac{k_B T}{q} \tag{3.6}$$

where k_B is the Boltzmann constant, T is temperature, and q is the magnitude of the elementary charge of an electron. From equations 3.5 and 3.6 it is clear that the current through a diode exhibits a non-linear temperature dependence. The non-linearity can, however, be rectified through use of a log-scale when analyzing data. Transistors also use thermal voltage as their temperature-dependent variable, but through a squared factor [56].

IC thermometers provide a highly-linear and sensitive output, are cheap, and have a very fast time response. Some issues with them though are their limited operational temperature range, active nature, and accuracy [47].

The use of diodes and transistors for invasive temperature measurements in brain is only a recent development. Kim et al. [57], out of Dr. Gluckman's Penn State neural engineering group, developed a probe using thin-film zinc oxide (ZnO) transistors deposited via nano fabrication techniques onto flexible polyimide substrate. The implant consisted of an array of eight transistors, roughly 100 µm $\times$ 5 µm. The reported maximum sensitivity was 40 mV/℃. This was claimed to be over four times better than traditional silicon transistor devices. The device was only characterized *in-vitro*, but showed promise for future use in *in-vivo* experimentation.

3.2.2 Non-invasive Devices

It is difficult to take direct measurements, temperature or otherwise, from brain because any damage done to neuronal tissue is harmful to the host. It is often unethical to use invasive implants on human subjects, though certain exceptions do exist. In many cases of patients with abnormal brain, it is not advisable to create additional tissue damage. For these reasons, neural engineers have worked to develop non-invasive methods and devices for measuring temperature in brain. The advantage is obvious: there is no damage being done to the subject's brain. The disadvantages, however, are what lead to the need for invasive probes in research and medicine. Non-invasive devices can lack the spatial resolution and accuracy needed for mapping very small, localized thermal gradients. They can also be very expensive, large, and inaccessible for use. Still, they are an important part of brain temperature research and one should be familiar with the various devices available

in the field.

One of the earliest effective thermal mappings of brain regions using non-invasive devices comes from Corbett et al. in 1997 [58]. The group used hydrogen proton magnetic resonance (MR) spectroscopy inside a 1.5 Tesla magnet to map temperature-dependent changes in H_2O resonant frequencies in 4 cm^3 volumes of live human brain. The measurements taken were able to show large temperature gradients from deeper to more superficial brain structures as well as baseline temperature differences between the frontal lobe and thalamus. The accuracy of the MR device was estimated to be ± 1 ℃. Different types of spectroscopy have been used by various other groups, achieving similar results. In 2001 Hollis et al. [59] used near-infrared spectroscopy (NIRS) to observe deep brain temperatures in new-borns. NIRS uses light absorption to monitor temperature differences. The basic premise is that higher temperatures absorb more light. The standard error was about 1 ℃. Alternative non-invasive techniques, like microwave radiometry, are available and have been employed in studies too [60].

3.2.3 Summary

Many options are available to neural engineers for designing a temperature sensor for brain. Invasive contact sensors are attractive for their spatial, temporal, and thermal resolution. They also offer exceptional sensitivity and accuracy. Non-invasive devices and techniques avoid damaging brain, but lack the accuracy of invasive devices and are often too expensive to be used outside of a clinical setting. To better characterize certain neural pathologies it is necessary to get as accurate, sensitive, and localized a temperature measurement as possible. In some instances, such as in the cases of patients with severe epilepsy, the benefits of such

measurements can outweigh the damage being done to brain from a chronic neural probe. In the next section, a novel design for a minimally invasive, implantable thermistor array will be presented as an effective new tool for neuroscientists seeking to take better localized temperature measurements in brain.

Chapter 4

Thin-film Vanadium Oxide Thermistor Array

After comparing the merits of all the sensors available, we decided that a thermistor would be the optimal choice for use in a highly localized, highly sensitive temperature probe. Our design utilizes work done by Basantani et al. [53] [54] [55] on thin through-film Vanadium Oxide (VO_x) thermistors originally purposed for infrared imaging. Working along side him, Dr. Horn and Dr. Jackson from Penn State, we developed a thermistor array designed for minimally-invasive, localized and very sensitive temperature measurements in brain. The device incorporates all of the principles of an effective biomedical implant and temperature sensor, and is the nexus between everything that has been discussed up until this point. This chapter will go over the array, its thermal characteristics, physical design, and complementary electronics. The finer details about its fabrication, implantation, and *in-vitro* characterization, however, will be discussed in the Experimental Methods and Results chapters.

4.1 Thermal Properties of Thin Through-Film VO_x

The 85 nm thin-film vanadium oxide thermistors have a high resistivity, ρ, but a low resistance relative to high TCR thermistors. This leads to a very sensitive device with low electrical noise [53] [54] [55]. The combination of high sensitivity and low noise is good for measuring small temperature changes in brain as the signal-to-noise ratio is high. This is accomplished by changing the design from a traditional lateral (in-plane) conductivity to one with through-film (out-of-plane), or vertically-integrated, conductivity as seen in the figure 4.1. This lowers the resistance $R = \rho l/A$, from several GΩ to about a MΩ. This is due to having a smaller length (l) and thickness (t) of active sensing material (see figure 4.2) while still using a high resistivity VO_x deposit. ρ for the thermistors is on the order of 10^3 Ω-cm [53].

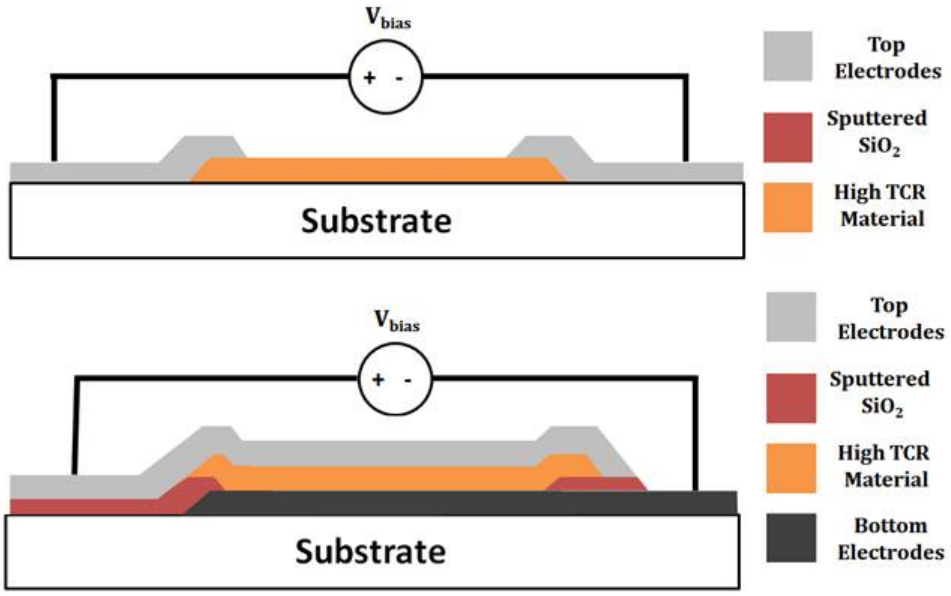

Figure 4.1: Cross-sectional views of lateral (top) and vertically integrated (bottom) sensors. The bottom electrode in the through-film sensor acts as ground for the V_{Bias} measurements. Credit: Basantani [53]

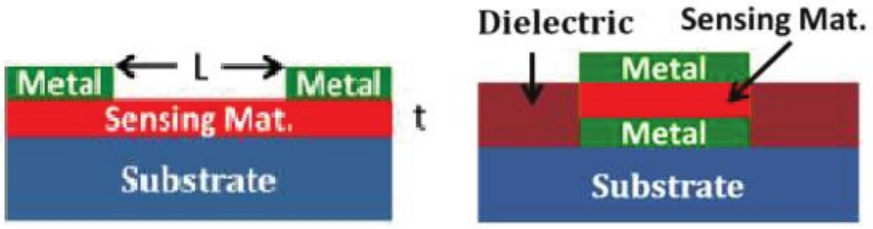

Figure 4.2: A comparison of lateral (left) vs vertically-integrated (right) resistance structures. The active sensor area for the vertically-integrated structure is significantly reduced. Credit: Basantani et al. [54]

4.2 Elements of the Array's Design

It is one thing to have an active sensing material that is well suited for measuring small temperature changes. It is another thing to transform that material into a fully functioning biomedical implant, specifically one designed for monitoring localized temperature field fluctuations in brain. The neural implant is not simply a temperature sensing device, but the combination of many different elements inclusive to the design. This includes: the physical layout of the array; the materials used for its substrate, wires, passivation, etc.; the interface electronics and acquisition system used to interpret resistance changes in the VO_x as temperature readouts; the implant materials and procedure; and the *in-vitro* testing platforms used to characterize the device.

4.2.1 Physical Layout of the Array

As mentioned in previous chapters, an effective brain temperature sensor must be able to resolve field changes on a spatial scale equal to or smaller than that of the neuronal cells and inter-capillary distances from which it is measuring. For this reason, careful consideration was given to the physical layout and dimensions of

the sensor. With Dr. Basantani's input concerning the capabilities of the nano fabrication machines and what would produce a high quality VO_x deposition, Dr. Gluckman and I determined how the array would be best laid out. The initial result can be seen in figure 4.3.

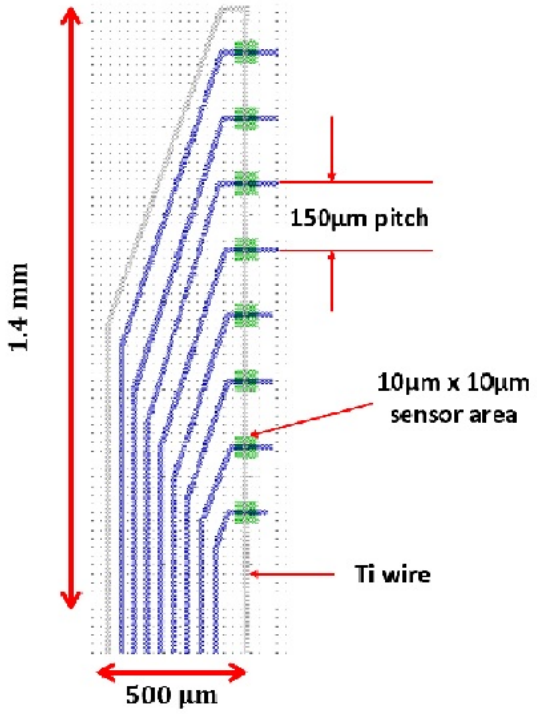

Figure 4.3: Schematic of the physical layout of the thermistor array. Active VO_x used for sensing is shown in green. The titanium (Ti) wire serves as the bottom electrode.

The active sensor area is 10 µm × 10 µm, which is smaller than most contact temperature sensor being used in the field and well within the range of intended spatial resolutions. The pitch between each sensor is 150 µm. This distance allows for recording of temperature gradients across neuron groups and capillary beds. The original design of the sensor leads called for a 90 degree angle to make the length shorter, but the mask program Dr. Basantani was using to fabricate the array could not initially support a good deposition of the wires' metal at that angle,

so 45 degrees was used instead. This problem was able to be overcome in later prints and can be seen in figures 4.4–4.5. The probes used in some of the sensor characterization, specifically in the bulk heat tests, were deposited at 45 degree angles.

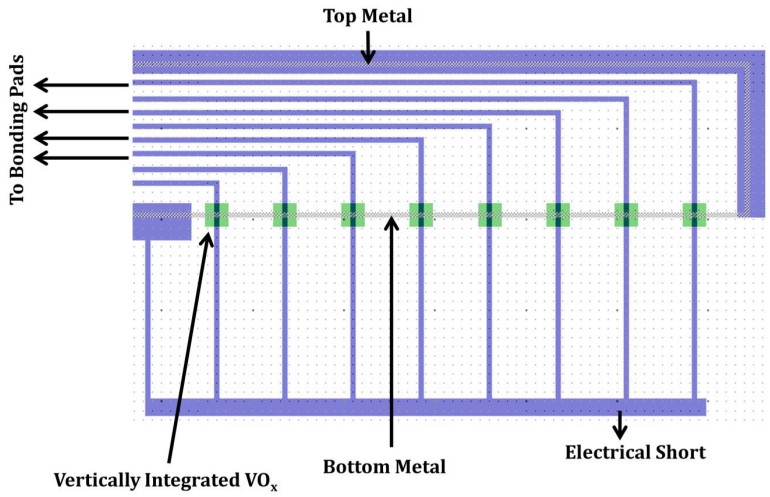

Figure 4.4: Thermistor array layout with a 90 degree deposition angle. The electrical short at the bottom is used for protection against electrostatic discharges (ESD). Credit: Basantani [53]

Figure 4.5: Magnified view of a 90 degree sample deposited on polyimide substrate.

In figures 4.4 and 4.5 an electrical short between the sensors is shown. This short protects the sensors from electrostatic discharge (ESD) during the bonding process (see Experimental Methods), as the active VO_x can burn out with as little

as 250 mV going across it. The spacing between each sensor still conforms with the 150 micron specification. The width of the array is also unchanged at 500 µm.

The thermistor array length is only on the order of a millimeter. The entire device though, which includes additional implanted material, is significantly longer. The sensor leads extend about another centimeter before spacing into a larger wire configuration where bonding to a wider polyimide ribbon takes place. These wires are used to connect the array to interface electronics. The probe can be placed at any depth within rat brain, which is approximately 11 mm thick [61], depending on the desired position of the recording. If, for example, an experiment called for a hippocampal recording, the sensors would have to be about 3-4 mm deep. This would leave roughly 2 mm of inactive polyimide and leads implanted in brain (see A.2 for a visual reference). Figures 4.6 and 4.7 show the full length of the device.

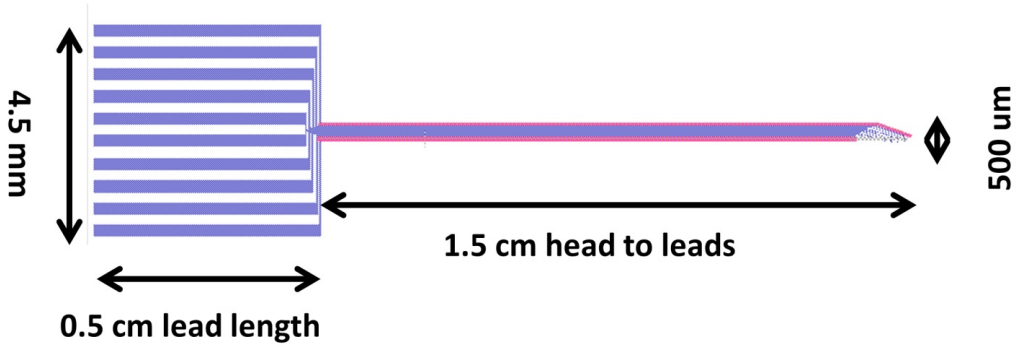

Figure 4.6: Schematic of the complete sensor leads. The layout of the wider wires are for connection to the interface electronics

4.2.2 Array Substrate

One of the most critical elements in the design of a neural implant is the substrate on which the sensors and leads are deposited. The substrate of a nano-fabricated device is often much thicker than the active material, thus influencing the physical

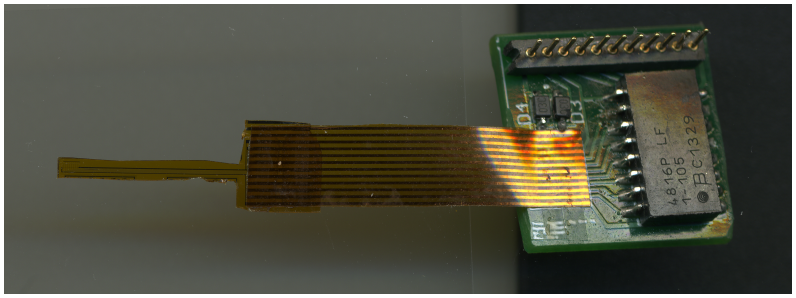

Figure 4.7: Complete view of the implant and polyimide ribbons. The smaller polyimide ribbon is bonded to the larger one connected to the circuit board.

dimensions and mechanical properties of the overall device. Some common materials used for neural implant substrates are silicon, metal, glass, and flexible polymers like polyimide, parylene, and PTFE. In the case of our array, glass and polyimide were used as substrates over the course of the design and *in-vitro* testing. While each type of substrate was useful toward the overall project, only one fit the end criteria for our design. Glass is not an ideal material for minimally-invasive, biocompatible implants and ultimately polyimide was the material chosen for the finished neural devices.

4.2.2.1 Glass

2 mm thick glass substrate was used for the 45 degree sensor lead deposits. Because glass of that thickness is stiff, deposition of the thin-film VO_x and 80 nm thick Ti leads was easier than if it were to be done on a thinner, more flexible material. Additionally, glass has good dielectric and thermal insulation properties. The sensors have a limited operation range and are very sensitive to ESD, so using glass helped protect them during heating and handling. For these reasons, glass worked well for much of the early array testing and proof of concept. Figure 4.8 shows a glass substrate array attached to a polyimide cable and interface board. Much of the printed objects on that glass sample are not part of the vertically-integrated

thermistor sensor array or testing, but are instead either lateral thermistors or ZnO transistor electrodes.

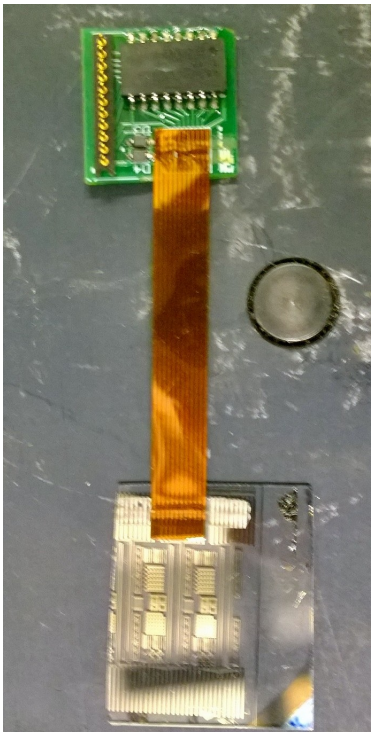

Figure 4.8: Array with glass substrate attached to an interface board.

As mentioned earlier, glass is not a suitable material for a minimally-invasive, chronic neural implant. This is for two primary reasons. First, glass has a large modulus of elasticity relative to brain. The mechanical mismatch would create excessive local damage and stress to the surrounding tissue. Second, while glass has been used before as an implant material, it is not very biocompatible over the long-term. In a seminal study done by Richardson Jr. et al. in 1993 [36], several candidate "biomaterials," including glass, PTFE, and polyimide, were compared for cytotoxicity, protein adsorption, clotting times, and hemolysis. The evaluation revealed glass to have poor chronic biocompatibility, making it not an attractive material for neural implants.

4.2.2.2 Polyimide

Polyimide is a flexible, relatively bio-inert family of polymers made from linked CO-NR_2 functional imide groups. Polyimides can be either thermoplastics or thermosets. They can be synthesized in several different ways, such as in condensation and addition reactions [36]. A famous example, and the type of polyimide used for our neural implant, is Dupont's Kapton. The molecular structure of Kapton can be seen in figure 4.9.

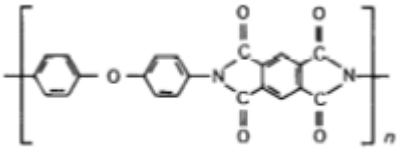

Figure 4.9: Molecular structure of Kapton. Credit: Richardson Jr. et al. [36]

Polyimide is very attractive as an implant substrate because of its mechanical, electrical, and biocompatible properties. The Young's modulus of polyimide is approximately 2.8 GPa [35] [39]. Recall that the modulus of elasticity for brain is about 3 KPa [31]. For comparison, silicon has a Young's modulus of around 169 GPa [62]. The lower stiffness gives polyimide a high flexibility. This aides it in adhering to brain tissue better as it pulsates with micromotion. Good electrical and physical contact can improve long-term recording stability and reduce the impact of an invasive device on surrounding tissue [37] [39] [41] [63] [64]. While polyimide is still stiffer than brain tissue, it is a significant improvement over traditional materials used for neural implants in terms of promoting chronic tissue health.

The downside of polyimide's high flexibility is the possibility of the substrate structure buckling upon insertion into brain. The buckling force of 20 µm polyimide was experimentally determined by Rouche et al. [39] to be 362 µN. This force is

too low for the thickness of most polyimide substrates in neural probes, as the maximum tissue force of brain has been measured as high as 1000 µN [35]. This creates a problem for the implantation of our 20 µm substrate device.

There are several possibilities for overcoming this problem. One method is to encapsulate the probe in a harder delivery shell that either gets removed or dissolves away. Takeuchi et al. [40] demonstrated that a thin encapsulation of flexible parylene substrate in polyethylene glycol (PEG), which is completely bio-absorbent in small amounts, could be used to add rigidity to neural implants. Their electrode array showed complete dissolution of the PEG shell and full recording capabilities present 200 seconds after insertion into brain-mimicking gel. Another solution is to provide the implant with structural support from a stiffer material, such as silicon or a metal. Lee et al. [38] used a 5–10 µm thick silicon backbone to assist their neural probe with a 20 µm polyimide substrate into tissue. This improved the probe stiffness by a factor of 13–20 whilst maintaining recording integrity. The backbone was permanently attached though, thus compromising chronic biocompatibility. Our solution was to combine these two methods and encapsulate our probe with PEG while using a temporary Si shuttle for quick and accurate implantation. More details about probe insertion into brain is discussed in the Experimental Methods chapter.

Polyimide is considered to be one of the best materials available for biomedical implants. Referencing Richardson Jr. et al.'s evaluation of biomaterials [36], polyimide showed great performance in many key biocompatibility tests. Results revealed polyimide to have low cytotoxicity, good protein adsorption, and clotting times 60% to 100% that of normal body response. A more recent 2007 study compared the biocompatibility of a platinum electrode and a polyimide substrate electrode. Surrounding tissue was better preserved by the polyimide. Additionally,

the toxic Pt electrode showed corrosion after chronic implantation, while the polyimide did not de-laminate in the harsh ionic environment of brain [41]. This result also supports the claim that polyimide does not worsen recording performance.

Overall, polyimide is well suited for the purposes of our array. Its physical properties and biocompatibility allow it to not interfere with recording performance or disrupt the surrounding biology much during long-term implantation. While it does need to be stiffened for the implant surgery, the temporary extra material, but smaller and more compliant chronic implant, is less damaging and less invasive than comparable devices that have Si or metal substrates.

4.2.3 Array Passivation

Array passivation is important for maintaining the health of an implant and the tissue surrounding it. A thin coating of biocompatible material can help prevent the device from becoming toxic to the local or global biology. It can also reduce the severity of immune responses, like fibrous encapsulation and tissue inflammation. From an electronics standpoint, a protective coating can be important for maintaining the quality of a sensor's measurements. In the case of thermistors, which lose sensitivity over time due to exposure, a passivation layer would help maintain original R_0 resistance and TCR values. The layer can not be too thick though, as it would inhibit detection of real-time temperature changes because of slower heat conduction and a greater time constant. Bio-inert polymers, like PTFE, polyimide, and parylene are commonly used as passivators for biomedical implants. For the purpose of our design, the material had to be easily deposited as a sealed conformal coating, highly biocompatible, mechanically similar to polyimide, and electrically insulating. Given these criteria, Parylene-C was chosen for the

protective layer of our array.

Parylene-C ($C_{16}H_{14}Cl_2$), or dichloro-paracyclophane, is a polymer known for its dielectric and low moisture permeability properties [65], chemical inertness, and low cytotoxicity. Parylene-C is a Class VI polymer in the United States, giving it the highest level of long-term biocompatibility for polymers according to the U.S Pharmacopeia [66]. Mechanically, parylene-C is comparable to polyimide. It has a tensile modulus of 3.2 GPa [67]. Additionally, it is easy to deposit in thin layers using a Gorham chemical vapor deposition (CVD) process, where temperatures do not exceed 600 ℃ [67] [68] and the process can be done in a few hours. For our array, CVD was used to deposit a thin 1–5 µm layer of parylene-C onto polyimide substrate arrays. In 2010, Lin et al. [66] demonstrated the viability of parylene-C as a passivation material by packaging their biosensor array with a 5 µm layer of the polymer. The device was exposed to a harsh piranha solution and then tested for electrical performance using cyclic voltammetry. The results showed the parylene coating did not interfere with the electrodes and insulated the biosensors from the external fluid. Overall, parylene-C is a quality passivation material that is well suited for the design criteria of our array.

4.3 Array Electronics

The sensor array cannot take temperature measurements on its own. It needs complementary circuitry to actuate the thermistors, acquire their voltage changes, and interpret samples of that data stream as real-time temperature fluctuations. In other words, the array is just one component of a complete acquisition system. Using the PSU EEG-8 data acquisition (DAQ) board created by Dr.Gluckman [69], I designed electronics to actuate the sensors via power from PSU EEG-8 and route

their continuous output to the PSU EEG-8 for signal amplification and digitization. The design of the circuitry takes into account several important factors, such as the burnout voltage of the thermistors and the physical size of the board layout so that it is compatible with free-motion recording from animals. A visualization of the overall acquisition process and the three circuit boards which make up the electronics can be seen in figures 4.10 and 4.11.

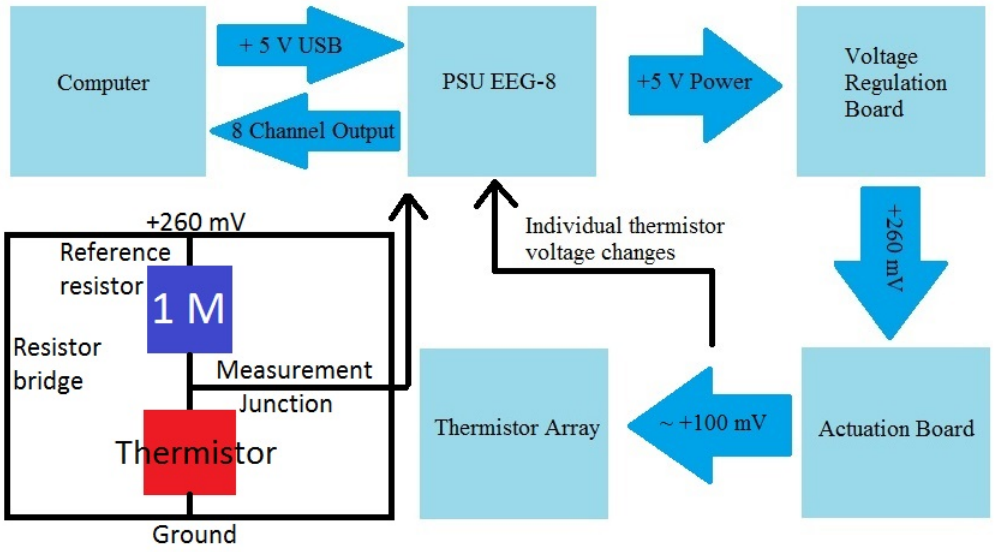

Figure 4.10: Flow chart of the complete acquisition system, from computer to array.

4.3.1 PSU EEG-8

PSU EEG-8 is an eight channel DAQ board purposed for biopotential recording. The board is designed to provide high-signal quality at a low cost. It takes advantage of open source software and several powerful IC components to provide a scientific grade DAQ board for around $100. For comparison, a commercial EEG recording system can go for a few thousand to tens of thousands of dollars. The board is divided into three sections: analog front end (AFE), microcontroller and power

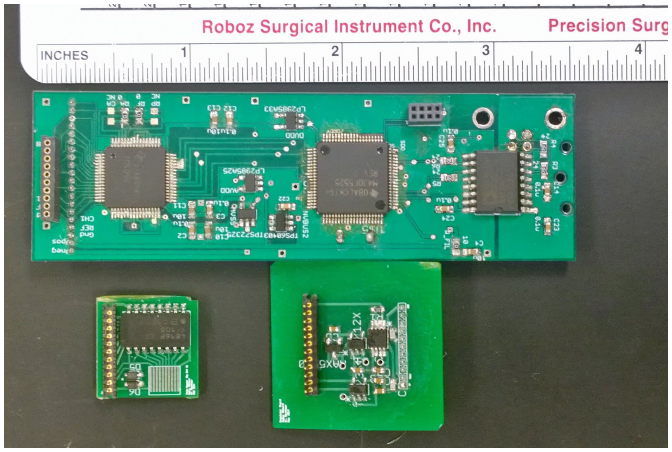

Figure 4.11: Circuit boards for the acquisition system. PSU EEG-8 is shown at the top. The thermistor actuation board (bottom left) and voltage regulation board (bottom right) are designed to interface the PSU EEG-8 to sensor arrays.

conditioning, and power and data isolation [69]. Details of the board's layout and architecture are shown in figure 4.12.

The flow of analog signals from sensor to computer is straight-forward. Our thermistor array will be used as an example to explain the process. First, changes in voltage move as eight individual channels into the PSU EEG-8 AFE where the ADS1299 uses 24-bit continuous Delta-Sigma analog to digital conversion (ADC) and built-in programmable gain amplifiers to decimate and amplify the signals. The now digital signals move to the MSP430 where data is sent over general purpose input/output pins using serial peripheral interface (SPI) communication to universal serial bus (USB) and into a computer. Data can then be imported and interpreted on the computer using commercial software or programming languages, like MATLAB, LabView, C, C++, etc. A custom LabView acquisition program written by Dr. Gluckman was used to read the sensor array data for this project.

One of the main goals of PSU EEG-8 is to provide "plug-and-play" capabilities for recording experiments. The system is designed to be a versatile research tool and helpful in situations where access to cumbersome and expensive equipment is

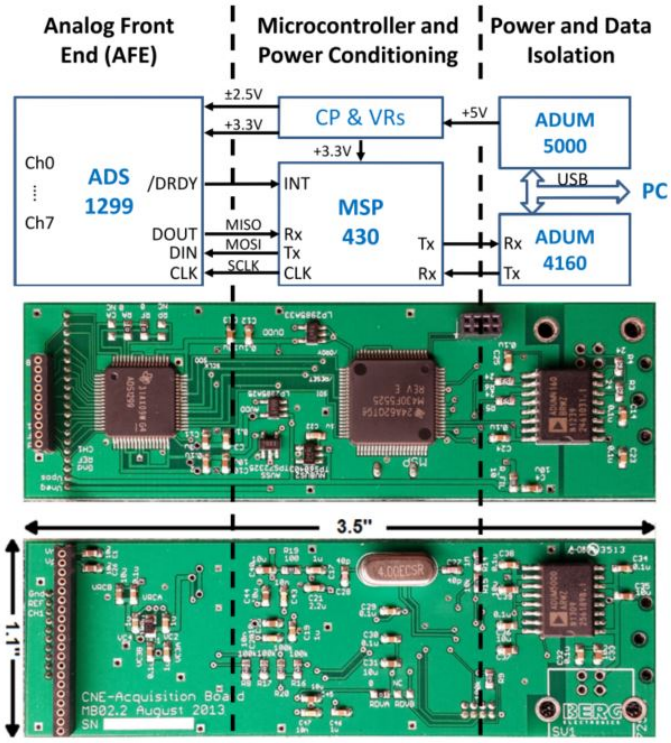

Figure 4.12: The complete PSU EEG-8 system. The board is sectioned into three parts. The analog front end uses an TI ADS1299 to amplify and digitize incoming channel signals. The TI MSP430 microcontroller communicates between the AFE and computer's USB via SPI. The ADUM 5000 and ADUM 4160 chips in the power isolation section protect the board and recording subjects from power surges upwards of 5000 Volts. Credit: Nabi et al. [69]

not available, such as remote medical clinics. With PSU EEG-8, one can simply deploy one or two modular circuitry attachments and be able to measure a wide range of biopotentials, including EEG, electrocardiogram (ECG), electromyogram (EMG), etc. The only extra pieces needed are a computer and program to import recording data. The easy use of our temperature sensor array with the DAQ system is a testament to design feature.

4.3.2 Acquisition Interface Circuitry

Two circuit boards were designed using CadSoft Eagle software to safely actuate the thermistor array and interface its outputs with the DAQ board. Dr. Basantani estimated that the sensors could burn out at voltages greater than 250 mV. The voltage regulation board is designed to deliver a safe potential to the thermistor actuation board. In reality, the two separate boards are a part of the same circuit. But due to the disposable nature of the implants and the need to permanently bond a polyimide ribbon to the electronics, the actuation board is a stand-alone piece. This is advantageous though, because the regulation board contains additional circuitry that can be used to calibrate arrays to which it is connected.

Another important element to the boards' designs are their physical dimensions. In order to perform *in-vivo* recordings on freely moving animals, the electronics need to be inside an enclosure close to the animal's head. I previously designed, using SolidWorks, a head mount for Dr. Gluckman's lab that can be 3-D printed and which houses EEG electrodes and head stage circuitry. This same head mount, seen in figures 4.13a and 4.13b, can also be used for the acquisition interface circuitry. The dimensions of the head mount are anatomically fit to a Long Evans rat skull (figure 4.14). This was accomplished by rendering and printing a computer-aided design (CAD) model of a skull from layering images. The actuation board is designed to hang below the regulator board inside the head mount, where the polyimide probe is guided from the bottom of the enclosure into an animal's brain (figure 4.15).

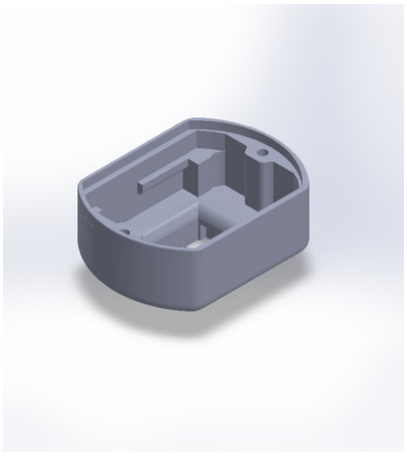

(a) Head mount designed to house implants and electronics. The bottom hole fits the average size of a Long Evans rat skull. Electronics lay on the special side wall and corner ledges. Implants feed out the bottom into the animal's head. The head mount is attached directly to the animal's head using dental cement.

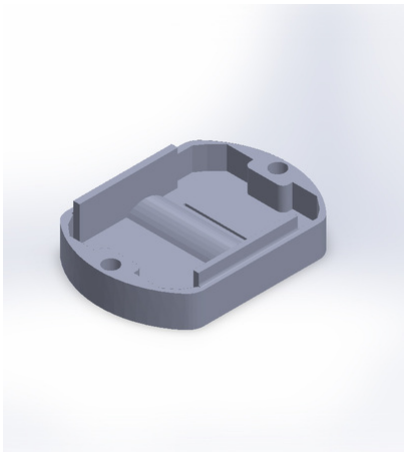

(b) Lid for the head mount. The bump in the middle is used to guide a small commutator ribbon that feeds out of the narrow slit on the top of the piece. The side protrusions are designed to apply even pressure to the electronics sitting inside the head mount and hold them in place.

Figure 4.13

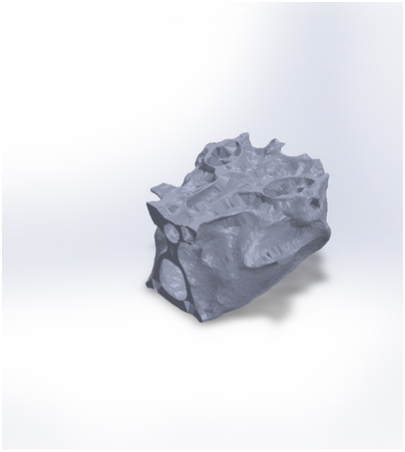

Figure 4.14: An anatomically correct 3-D model of a Long Evans rat skull. The skull model was rendered using Visio and then imported into SoldiWorks for later printing.

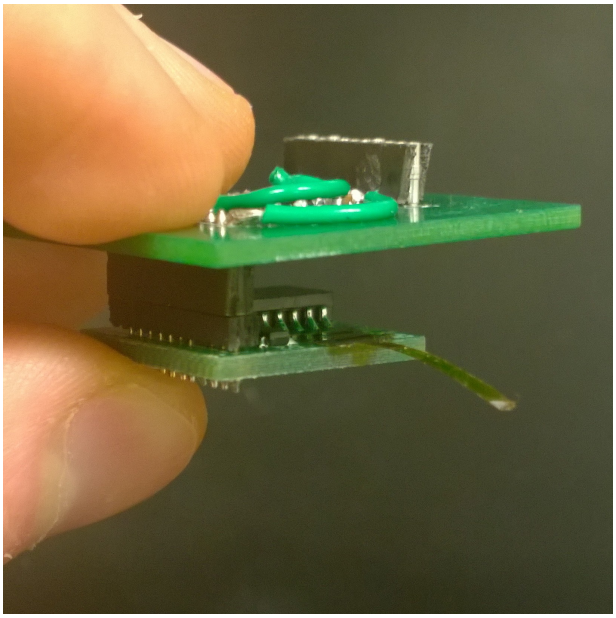

Figure 4.15: The two boards attached via Mill-Max pin connectors. This configuration sits inside the head mount with the polyimide probe (which would have a much longer ribbon cable attached to it for actual implantation) going out of the bottom and into the animal's brain.

4.3.2.1 Voltage Regulation Board

The voltage regulation board is the main piece interfacing the array to PSU EEG-8. It takes +5 V and ground (GND) from the DAQ board and reduces the magnitude of that voltage to 260 mV. This final output voltage, which serves are the input for the actuation board, is well within the 250 mV limit after it drops across the 1 MΩ resistors on the actuation board. There are two main ICs on this board, the TLV712 and the ADG823. The TLV712 is a Texas Instruments 1 V, 0.3 A voltage regulator [70]. It reduces the +5 V input signal to a stable +1 V output, which then goes to a resistor bridge where it gets reduced further down to 260 mV. The ADG823 is an Analog Devices dual switch [71]. This switch is purposed for connecting a local ground signal (H+) that can be used to calibrate sensor arrays. I made the footprint for the switch myself using Eagle's library design tool to match

the physical dimensions and pin connections specified by the chip's data sheet. For this project, however, the sensor calibration switch was not employed. The eight channels carrying the voltage signals from the thermistors are routed from the bottom of the board directly to the top connector landing where the regulation board connects to PSU EEG-8. A schematic of the circuit is shown in figure 4.16 and the layout of the board is shown in figure 4.17a. The actual board used for all the testing is shown in figure 4.17b.

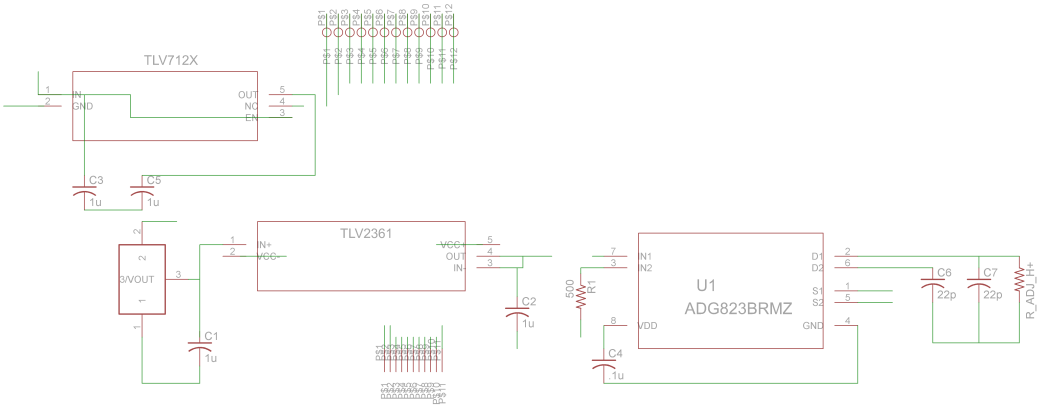

Figure 4.16: Schematic of the voltage regulation circuit. The wires are not physically connected because they are labelled and thus connected in Eagle. The physical layout of the schematic has no bearing on the board layout. TLV2361 is a unity gain op amp intended to match impedances from PSU EEG-8 to the actuation board. The IC was not functioning as intended though, and ultimately was not used in the working board used for testing.

4.3.2.2 Thermistor Actuation Board

The thermistor actuation board is the final piece of the interface electronics. It takes the 260 mV signal from the regulation board and moves it across eight parallel resistor bridges. Each bridge is comprised of a 1 MΩ resistor and a thermistor. The voltage drop across the thermistor, represented by equation 4.1, is measured and routed to eight pins that correspond to the eight channels the DAQ board

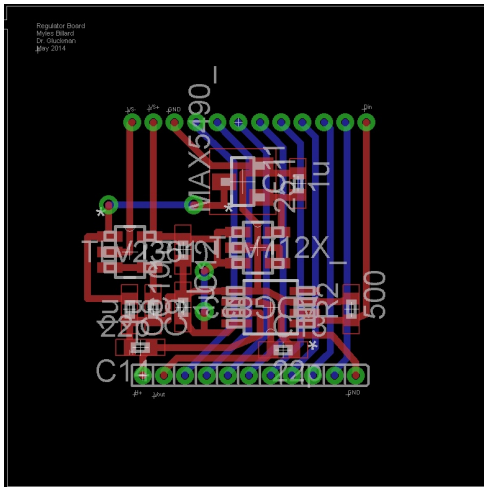

(a) The voltage regulation board layout. Power from PSU EEG-8 comes into the top connector landing. Individual channel signals also go out to PSU EEG-8 from that connector. The bottom connector landing attached the regulation board to the actuation board and has pins for H+, the 260 mV power signal, the 8 thermistor signals, and ground. The red and blue wires represent the top and bottom layers of the board, respectively.

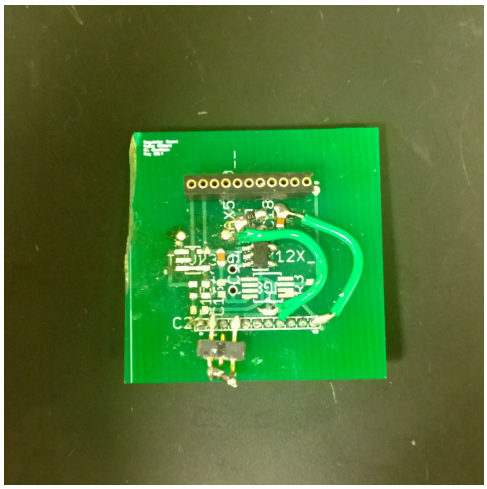

(b) The board used for all the in-vitro testing done in this project. The TLV2361 and ADG823 were removed and wires were soldered to the appropriate places to establish Vout and GND connections.

Figure 4.17

uses. The circuit also contains a pair of oppositely oriented diodes that protect the sensors from ESD. On the board are ten 50 µm pitch, 0.5 cm length surface mount device (smd) pads used to bond the board to the polyimide ribbon. The circuit's schematic and board layout are shown in figures 4.18 and 4.19 and a fully fabricated board is shown in figure 4.20.

$$V_{out} = V_{in}\frac{R_2}{R_1 + R_2} \tag{4.1}$$

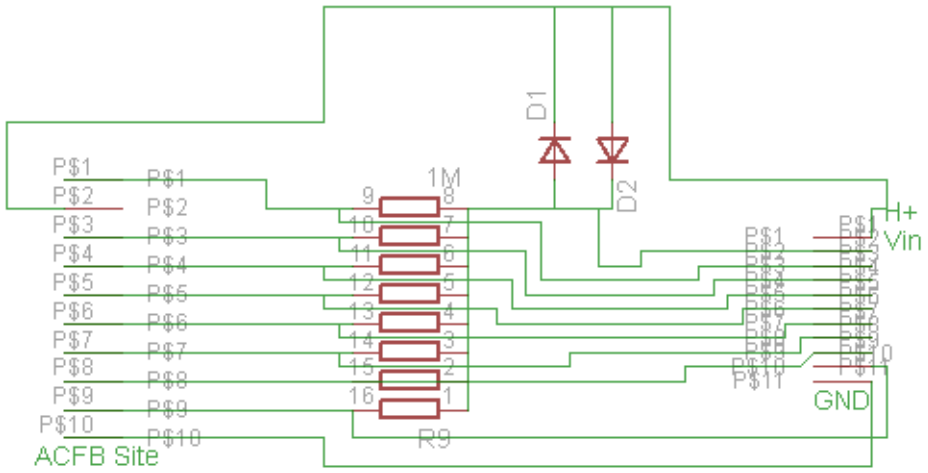

Figure 4.18: Schematic of the actuation circuit designed in Eagle. The pins connecting this to the regulation board are on the right. The Vin signal is moved across individual resistors to the ACFB site, where the smd pads are.

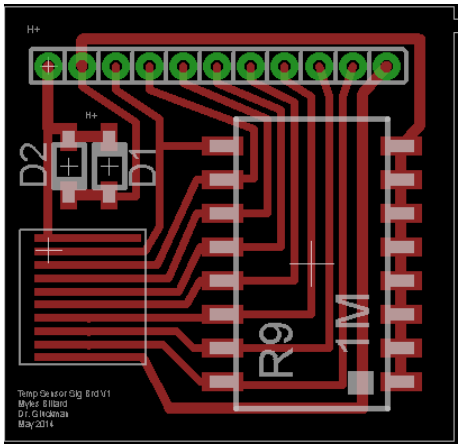

Figure 4.19: Board layout of the actuation circuit. The individual 1 MΩ resistors are a part of the R9 chip. Measured thermistor voltages are routed from the pins of R9 where the 1 MΩ resistor ends to the connector landing at the top of the board. H+ is the local ground wire that will be used for sensor calibration.

4.4 Summary

The VO_x thermistor array that was presented in this chapter is at the forefront of implantable neural engineering technology. Each of its design elements come together in a minimally-invasive, biocompatible, and very sensitive device purposed

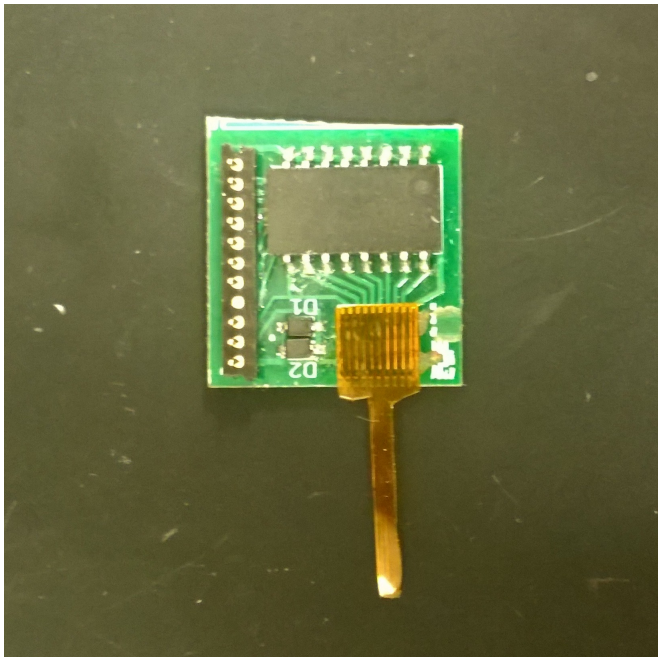

Figure 4.20: Complete thermistor actuation board with polyimide ribbon bonded to the smd pads.

for taking highly localized temperature fields measurements in brain. The spatial and thermal resolution that the array offers surpasses that of most contemporary temperature sensors being used in the field. Features from our plug-and-play acquisition system, which include additional interface electronics to safely actuate the sensors, routing of the measurement signals, and the ability to calibrate the thermistors, make our overall set up, from implant to computer, robust and easy to use. The next two chapters are Experimental Methods and Results. There the testing and characterization of the system, including measured thermistor resistance and sensitivity, as well as the recording electronics performance, will be presented.

Chapter 5

Experimental Methods

The next two chapters, Experimental Methods and Results, are where our system and its design choices are validated. The Experimental Methods chapter, specifically, covers the following material: fabrication of the VO_x array; attachment of the array to the interface electronics; design of testing platforms used to characterize the performance of our system; and development of the procedure for surgical implantation of the probe. These pieces are at the center of this entire engineering project, and the success of the temperature array as a viable tool for neurological studies depends on the results of these experiments.

5.1 Fabrication of Complete VO_x Implants

The fabrication of the complete temperature sensing implant is comprised of three main components: the VO_x thermistor depositions, anisotropic conductive film (ACF) bonding of the array to the acquisition electronics, and parylene-C passivation. The first process was done by Dr. Basantani for this project, while the second was done by me with guidance from him and students of Dr. Jackson's thin-films group. The array passivation was completed with the help of a Mr.

Chindam, a graduate student from Dr. Lakhtakia's lab. The performance of the overall system was greatly determined by the outcome quality of these procedures. In some fabrication samples, the sensor leads got micro particles, such as dust or Ti deposits, embedded on and between them and ended up fractured or shorted, which resulted in disconnected channels. During bonding, some samples and actuation boards had to be discarded because of misaligned or poor electrical connections. Overall though, successful fabrication of a complete device takes about three to four days.

5.1.1 VO_x Thermistor Deposition

Deposition of the vertically-integrated thermistors was done using Biased target Ion Beam Deposition (BTIBD), which incorporates nano fabrication techniques of sputtering and wet-etching. The procedure was done at the Penn State Millenium Science Complex nano fabrication facilities. 85 nm thick VO_x and top and bottom 80 nm titanium lead deposits were made on either 2 mm thick glass substrate (figure 4.8) or 20 µm polyimide substrate. The deposition process is shown in figure 5.1. A sample deposited on polyimide is shown in figure 5.2. One important point to note is that the TCR of the active VO_x material is controlled by the oxygen content in the chamber during BTIBD. From start to finish, a clean deposition process takes about 20 hours to complete. Though during the time course of this project, Dr. Basantani ran into equipment troubles on more than one occasion, especially during deposition of the VO_x. Those issues delayed fabrication of the arrays, sometimes by a week or more. A complete explanation of the deposition process can be found in Dr. Basantani's 2014 PhD dissertation [53].

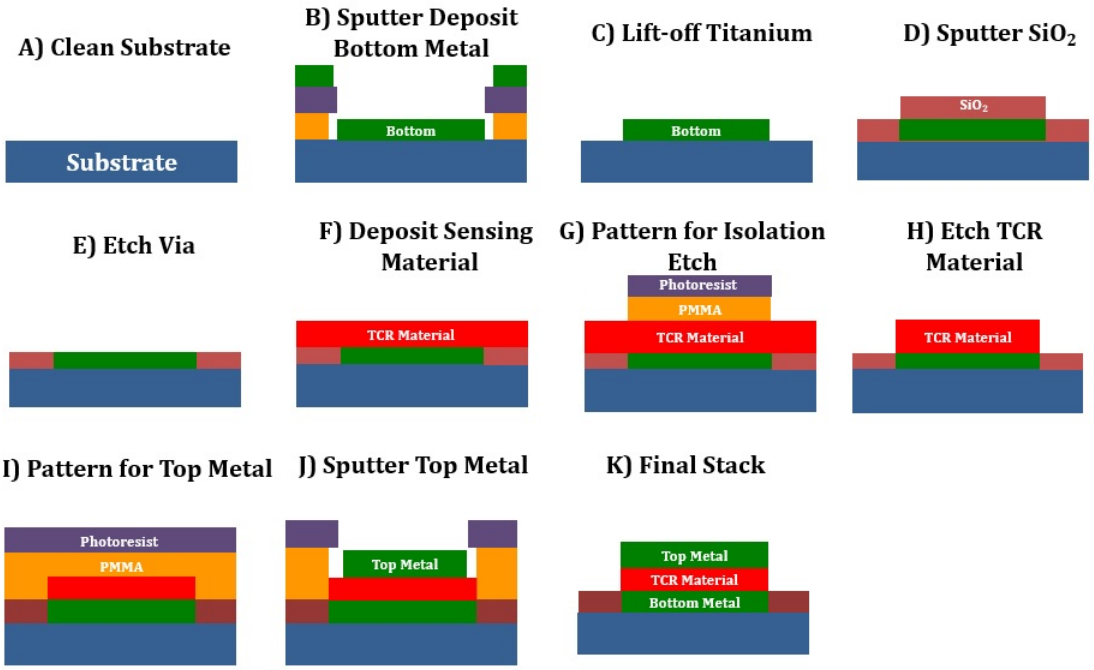

Figure 5.1: Work flow process of VO_x and Ti lead sputter deposition onto substrate. For the through film thermistors a wet-etching process had to be used, as dry etching destroyed the VO_x. This is a just a visual representation and the pieces are not to scale. Credit: Basantani [53]

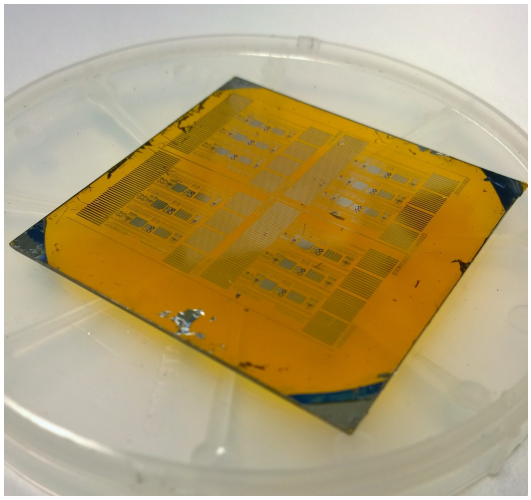

Figure 5.2: Array samples deposited on 20 µm thick polyimide substrate. The polyimide substrate is sitting on a thicker piece of glass to make cutting out the sensors and leads easier.

5.1.2 ACF Bonding

ACF bonding is process by which circuits, typically flexible electronics, can be electrically connected to other circuits. ACF bonding was performed using Hitachi ANISOLM AC-7206U-18 ACF Film [datasheet not available], a thermosetting polymer. Titanium leads from the array deposits were bonded to a 2 cm long Kapton ribbon with ten 50 µm pitch copper wires. The bonding process was done under a microscope using a heated press that melts the film to about 150 ℃ while pressing the aligned wires together. After the maximum bonding temperature has been reached, it takes 30–60 seconds for the melted film to set and a firm physical and electrical connection is established. Figures 5.3 and 5.4 show the results of two ACF bonded arrays, with the bonding sites highlighted. The electrical short used to protect the sensors from ESD during this process (figure 4.4) was cut immediately afterwards.

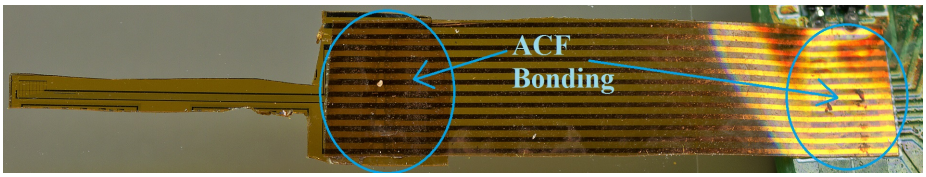

Figure 5.3: Post ACF bonding of an array to a polyimide ribbon to an actuation board. The adhesive can be seen in the highlighted areas.

5.1.3 Parylene C Passivation

The preparation and deposition process of parylene-C used for our arrays is a common technique that was first established by Gorham in 1966 [68]. Parylene-C dimer is first vaporized at 175 ℃ and then put into a furnace where it is heated to 600 ℃. At that temperature the dimer pyrolizes, or dissociates, into a monomer. The monomer vapor is then passed into a cooler vacuum chamber in which the

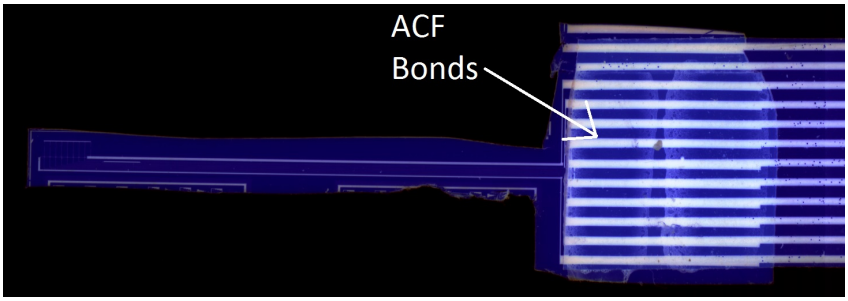

Figure 5.4: A high contrast image of an ACF bond. Slight misalignment of the wires can be seen in the bonding area, though it was accurate enough to not affect the electrical connection of the sensors to the ribbon.

sample to be coated sits. There it condenses over the sample as a uniform coating. Our arrays have a 1-5 µm thin-film passivation layer. At that thickness, the material has mechanical properties similar to Saran wrap or similarly thin polyimide. The coating is transparent, so it cannot be seen on an array. Figure 5.5 though shows a parylene-C sample taken from a run of the deposition process.

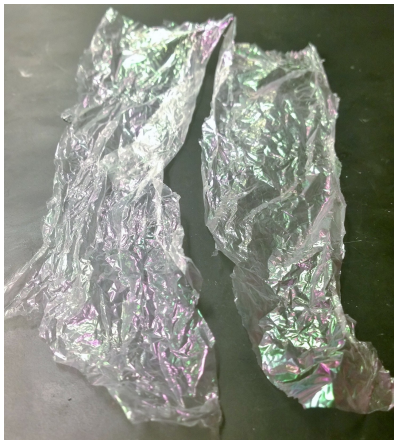

Figure 5.5: An 1–5 µm thick thin-film parylene-C sample taken from the Gorham deposition process.

5.2 In-Vitro Testing

Before the arrays can be used for invasive recordings, they must first be tested and validated with *in-vitro* experimentation. This section focuses on experiments used to characterize the thermal properties of the VO_x, like TCR and thermistor resistance, and to test its ability to measure small temperature gradients and record whilst immersed in a liquid environment. The TCR and bulk heat testing was done using glass substrate. The thermal gradient and immersion testing will and was done using polyimide samples. *In-vivo* testing of the array was beyond the scope of this project, but will be a part of my Master's thesis. The *in-vitro* experiments are designed to prove its potential as a high-functioning neural implant designed to measure small, localized temperature field dynamics in brain.

5.2.1 TCR Testing

Pre-ACF bonded glass substrate samples were tested on a hot plate electrical probe station for resistance and TCR characterization using Dr. Jackson's equipment. First, a several nA current was sent across individual thermistors to check for electrical shorts or deposition mistakes. Afterwards, one thermistor from each sample was used in hot plate testing for resistance measurements and TCR calculation.

In the hot plate experiment, temperature began at room temperature (20 ℃) and was continuously increased to a maximum temperature of 57 ℃ while resistance was sampled at discrete, non periodic intervals. The resistance measurements were then exported into an excel workbook. Calculations to solve for the activation energy, E_a, of the thermistor and extract the approximate TCR of the sample were then performed using MATLAB. E_a can be approximated as the slope of the best

fit line plotted from ln(R) vs $1/k_BT$ and the TCR can be calculated from equation 3.4.

5.2.2 Bulk Heat Testing

After ACF bonding glass substrate samples to the actuation board, bulk heat testing was performed using the complete acquisition system. The goal was to calculate actual sensitivity of the sensor array by measuring resistance change over a specific time domain in a configuration similar to what would be experienced outside of the initial TCR testing. A VWR Heating Block, designed for heating test tubes, was used to heat an insulated chamber to various temperature set points. Voltage measurements from the eight channel array were recorded using LabView. The testing set up can be seen in figures 5.6–5.8.

Figure 5.6: View of the computer and foam-insulated heating block used for the bulk heat testing. The array and interface electronics sit inside the chamber. The DAQ board sits outside the chamber. A foam lid was placed on top of the chamber for the tests.

Several minutes of recording at room temperature were done to determine R_0 and to see which channels were working properly. The heating block was then set

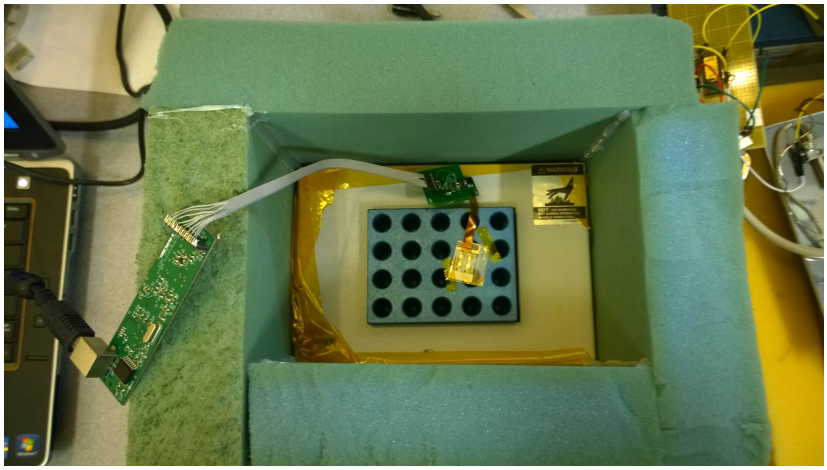

Figure 5.7: Picture of the bulk heat test set up, from sensor array to USB output. The glass substrate sample was taped down during testing because the connector cable was torquing the set up.

Figure 5.8: An up close image of the heating block with the sensor array and interface electronics.

to 30 ℃ to visually observe how the sensors responded, as well as see how long it took for the temperature to stabilize at that set point. After several minutes the set point was changed to 35 ℃. The system was then left alone for several hours to record. After a while the set point was changed to 40 ℃ and left alone again. Upon completion of the experiment, binary files of recorded data were imported into MATLAB for post-processing and analysis.

5.2.3 Thermal Gradient Testing

Our thermistor array is designed to measure small, localized temperature gradients in brain. A heating bridge circuit board was created to test this specific ability. This section includes both the design and background of the heating bridge circuit, to understand how and why it works, and the design of the thermal gradient experiment that will be used to analyze how well our complete temperature device performs in one of its most essential tasks. Experimentation could not take place before the deadline of this thesis, though the circuit board has been printed and LabView code is being written to make it function properly for gradient testing.

5.2.3.1 Heating Bridge Design

The circuit schematic and board layout, as well as the soldered board that will be used for gradient testing, can be seen in figures 5.9–5.11.

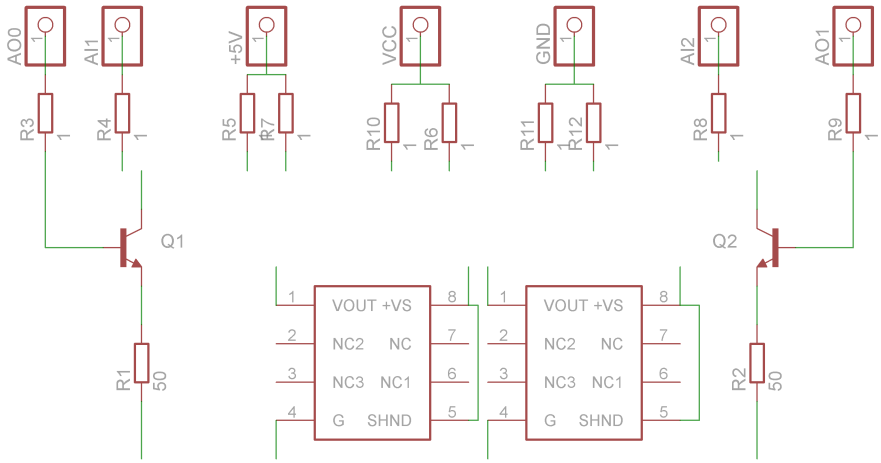

Figure 5.9: Heating bridge circuit schematic. Pin outs at the top allow input power to the board's components and output signals to a LabView 6211 NI-DAQ card. 1 Ω resistors are placed as a buffer between the pins and the board to prevent heat dissipation through the wires. Q1 and Q2 are transistors. The 8 pin symbols in the middle are the TMP37, which I designed myself using Eagle.

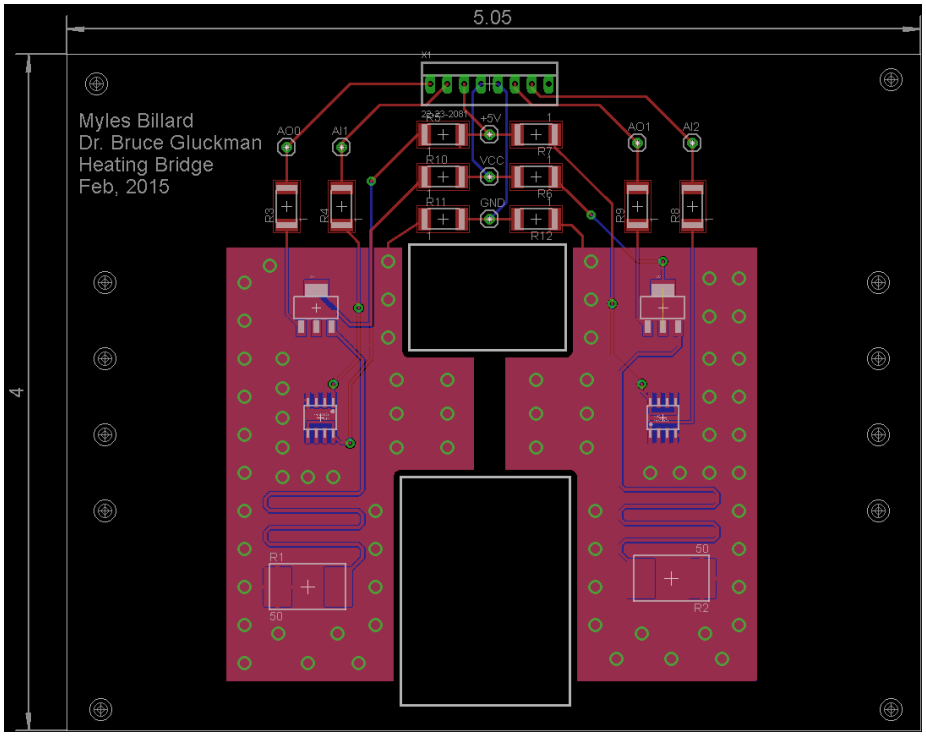

Figure 5.10: Layout of the heating bridge board. The filled in red and blue areas are the top and bottom Cu ground plates. The green circles are vias, or tin-plated holes, that allow thermal conduction between the top and bottom layers. The FR4 bridge is at the center of the board.

The heating bridge uses Fairchild PZT3904 NPN bipolar junction transistor [data sheet not available], 50 Ω wire-wound power resistor [72], and Texas Instruments TMP37 IC temperature sensor [73] components to heat top and bottom layers of 35 µm thick 1 oz copper ground plates on each side of the board. Controlled heating of each side will be done using a proportional-integral (PI) controller. Temperature measurements from the TMP37 will be used as part of a feedback loop. The analog voltage outputs from the chips will be compared to set points for desired plate temperatures. Difference errors between the values will be used to calculate a real-time adjustments of respective V_b magnitudes via analog output from the NI-DAQ card. This will control the flow of VCC current through the transistor

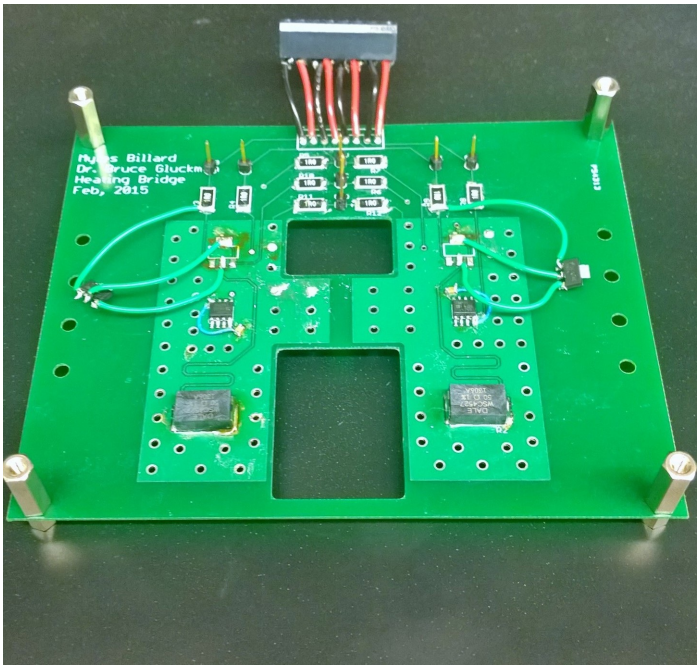

Figure 5.11: Heating bridge with soldered components. Two modifications were made from the original layout. A 0.1 µF capacitor was added from Vin to GND on the TMP37 to stabilize input power and the transistor had to be soldered to different pins because the collector and emitter pins on the footprint were connected backwards. The transistor, TMP37, and bottom resistor will all be thermally potted to the copper ground planes for quicker conduction of heat from the components to the board.

junction and 50 Ω resistor. At steady-state power dissipation heat flux between the components, the board, and the external environment will be constant. This will stabilize temperatures of the Cu plates very close the desired set points.

If successful, the PI controller will stabilize a temperature field across the bridge at the center of the board. The heating bridge is a 0.5 cm wide FR4 (material used for PCB lamination) strip with two board cut outs on either side. At different temperatures, the Cu plates, which absorb heat dissipated from the transistors and power resistors, create a thermal conduction gradient between them. The heat will diffuse from the higher temperature heat source to the lower temperature one according to Fourier's 1-D heat conduction equation equation 5.1. Thermal flow

will primarily be across the FR4 bridge due to the large cut outs which, while the board is in rough vacuum, will impede conduction in the vertical directions. This is because vacuum does not conduct heat as well as the FR4.

$$q = -kA\frac{dT}{dx} \tag{5.1}$$

q is heat flux

k is in-plane thermal conductivity

A is area

dT/dx is change in temperature per unit length

In-plane conductivity of FR4 is 0.3–0.4 W/m-K [74]. Area is that of the bridge, which is 0.5 cm × 1.75 cm. At steady-state (i.e q = constant), the conduction gradient will have continuous, uniform temperature change in the x-direction. Set point adjustment will be able to control the resolution of temperature change down to the mK/µm scale for testing of the array.

5.2.3.2 Thermal Gradient Experimental Set Up

All thermal gradient testing will be done in an evacuated Pyrex bell jar. Wires will run from stopped holes underneath a raised platform out to the NI-DAQ 6211 and a +10 V power supply. The transistors, TMP37s, and bottom resistors will all be thermally potted to the copper ground planes for quicker thermal conduction from the heating components to the board. The PI controller will stabilize Cu plate temperatures and recording will take place. After sufficient time has passed, the set points will be changed and recording will continue. Data will be exported into MATLAB for analysis.

5.2.4 Immersion Testing

A passivated polyimide substrate array was immersed in an inexact volume of 0.9% NaCl H_2O saline solution in a 100 mL glass beaker at room temperature. Temperature measurements were recorded. About ten minutes of data were taken at room temperature to begin the recording. Afterwards the hot plate was turned on to at set point of 60 ℃ until the bath temperature reached approximately 35 ℃, upon which the hot plate was turned up to a 80 ℃ set point. It stayed at this set point over the next 20 minutes until the remainder of the experiment. The somewhat careless temperature changes were done because the hot plate is not very accurate, but the main goal of this test was to simply show recording capabilities of a passivated array when completely submerged in an ionic liquid environment.

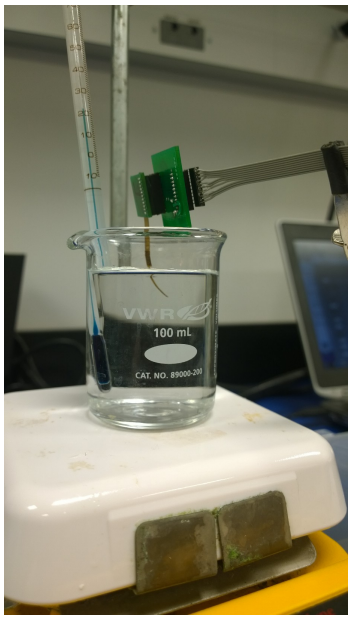

Figure 5.12: Passivated polyimide substrate array immersed in saline solution. The saline bath is heated on a hot plate.

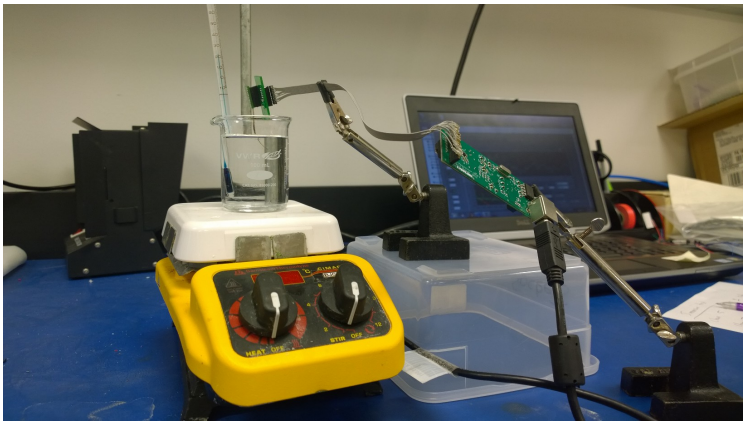

Figure 5.13: Complete view of immersion test set up.

5.3 Array Implantation

As discussed previously, the thin polyimide substrate is too flexible to be inserted into brain alone. It buckles from the tissue forces. To overcome this problem, but still trying to make the implant be as minimally-invasive as possible, we used PEG encapsulation with a removable silicon shuttle to assist the device during implantation. The system was then tested in an agarose gel to simulate implantation in living brain tissue. PEG encapsulation and agarose preparation guidelines were taken from previous work done in 2011 by Burak in Dr. Gluckman's lab, with some practical modifications [75].

Agarose gel, or simply agar, is a useful material for implantation simulation. At 0.6% concentration, it has similar mechanical properties to that of superficial brain tissue [76]. It is also homogeneous and transparent, making the experiment very reproducible and easy to observe. A 20 mL solution of 0.6% Type-III A agarose powder (0.12 g) [77] was prepared using deionized water in a 100 mL glass beaker. The powder was stirred into the water and put into a microwave oven on the high setting for one minute. The beaker was taken out and swirled gently every 15

seconds. After the full minute the solution was stirred again, then put back into the microwave for 45 seconds. The solution was stirred one final time, allowed to sit for two minutes, then placed into an "artificial brain tank" to set. Solidification occurred in about an hour at room temperature. The results are shown in figure 5.14. The artificial brain tank was designed using two glass microscope slides and a 3-D printed piece that I made in AutoCad. The tank has the advantage of being clear, so the results can be observed, and big enough for multiple implantations to take place in unbroken agar.

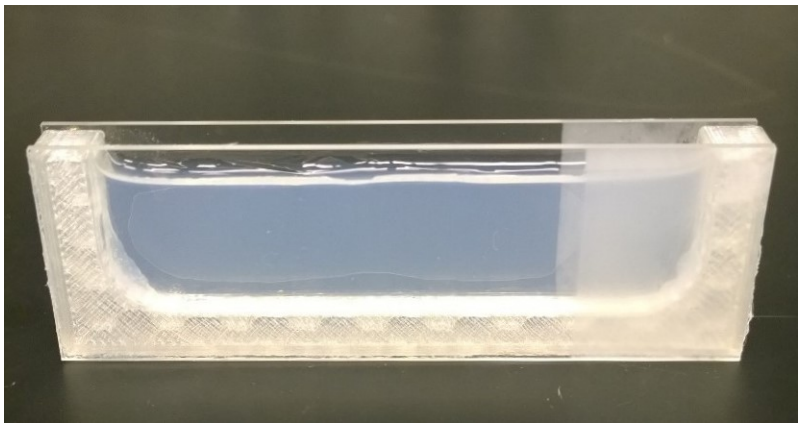

Figure 5.14: Artificial brain tank used for implantation tests. Two glass slides were attached to the 3-D printed plastic piece using room temperature vulcanization (RTV) epoxy. The agar gel inside will be used to simulate living brain tissue during implantation.

The silicon shuttle used for implantation assistance is made from a 25 µm thick (1 1 1) Si wafer. The wafer was diced into 2 cm × 1 mm rectangles by a laser cutter. Two samples can be seen in figure 5.15.

For the encapsulation process, a small amount of PEG, which is solid at room temperature, was heated in a 10 mL glass beaker at 120 ℃ for ten minutes. After melting, it was cooled and then maintained at 80 ℃, where it remained in liquid form, for the duration of implantation testing.

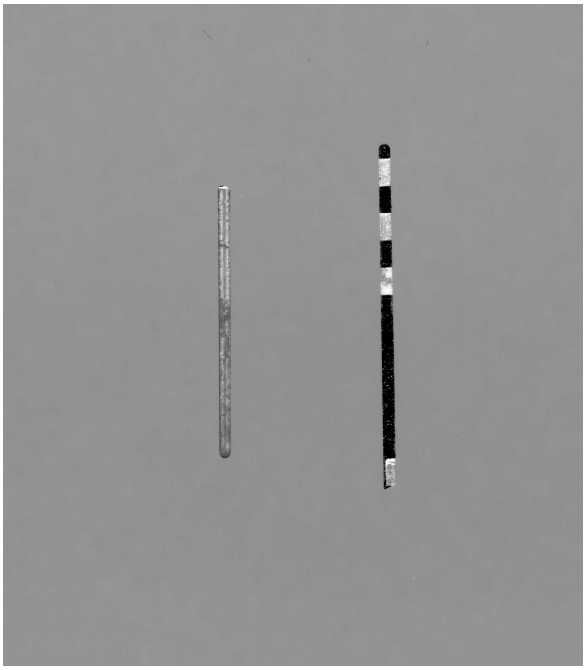

Figure 5.15: Grey scale image of two Si shuttle samples. The insertion side of the shuttles have the rounded tips. Cleavage of these samples are shown on either side with a 45° break

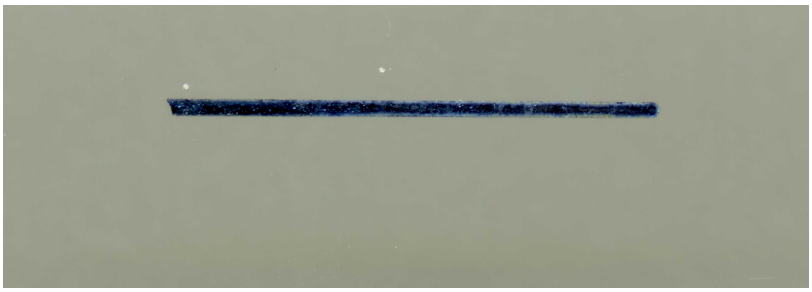

Figure 5.16: Colored image of another Si shuttle. The insertion side is to the right.

The dipping of the shuttle was done slowly by hand. A thin layer of PEG was applied to the shuttle in a first dip. This layer was used to help the array stick to the shuttle. After about 10 seconds the PEG dries, so quick and accurate placement of the implant is critical. A second dip was then performed to fully encapsulate the array in PEG. After the PEG dried, the Si shuttle was implanted into the artificial brain tank. The shuttle remained in the gel for approximately 30 seconds to allow

the PEG shell to dissolve, after which it was removed, leaving the implant behind.

Chapter 6

Results

6.1 TCR Testing

Figures 6.1 and 6.2 from TCR testing show the thermistor resistance of two glass substrate samples to be 1.304 MΩ and 450 kΩ with a TCRs of -4.04 %/℃ and -4.53 %/℃, respectively. An important nuance of calculating the TCR with equation 3.4 is that K_bT must be in units of electron-Volts (eV), so the K_b used was 8.617 x 10^{-5} eV/K. Voltage vs current and resistance vs temperature data from the first sample are shown in figures 6.3 and 6.4. MATLAB code written to import column the data from Microsoft Excel and to calculate E_a, TCR, etc can be found in Appendix B.

6.2 Bulk Heat Testing

Recordings from two separate bulk heat tests can be seen in figures 6.5 and 6.6. Recordings were post-processed in MATLAB using a 55–65 Hz stopband and 6 Hz low pass Butterworth filter to eliminate excessive 60 Hz noise and clean up the DC signal. The main code used to read, process, and plot the data files from these recordings can be found in Appendix B. The goal for the first recording was to show

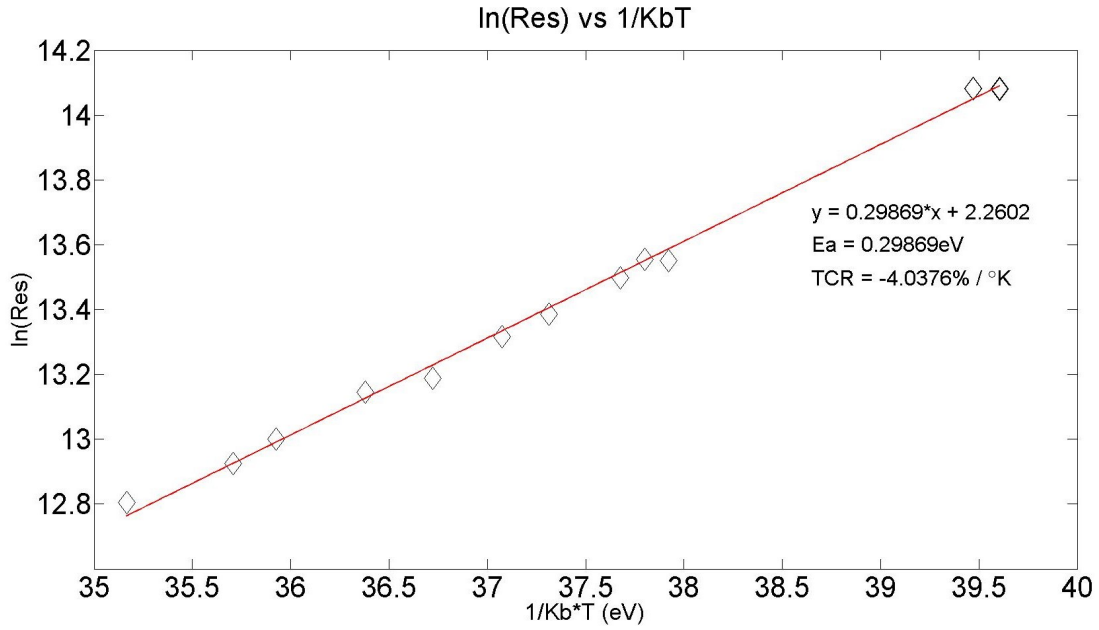

Figure 6.1: Data from TCR testing showing E_a and TCR of a sample thermistor on glass substrate. E_a is the slope of the best fit ln(Res) vs $1/k_BT$ line and is 0.299 eV. TCR is calculated as -4.04 %/K

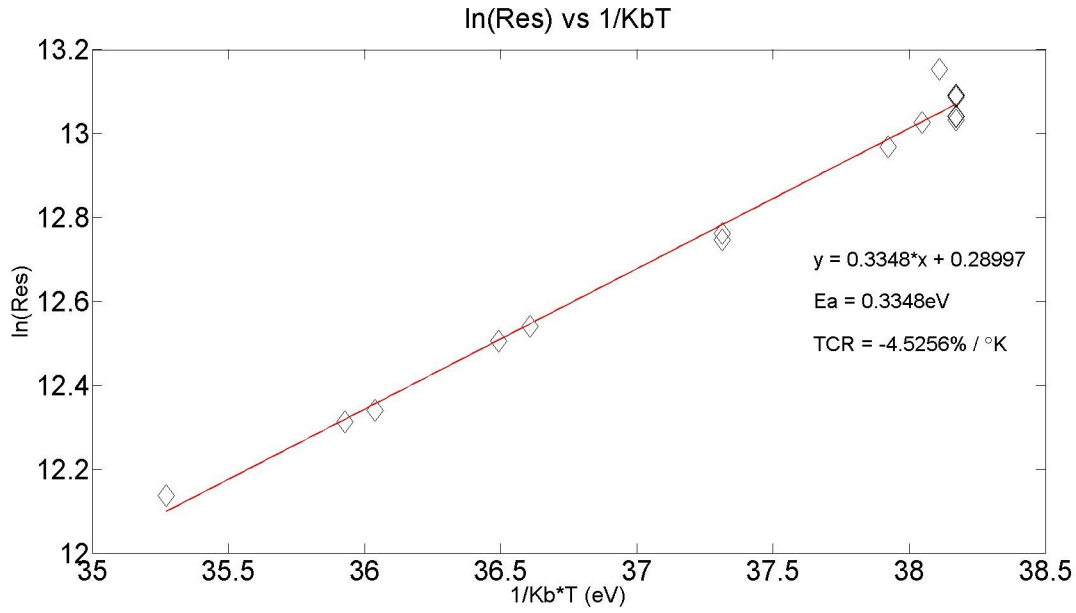

Figure 6.2: TCR testing data from a second sample. The TCR magnitude of this thermistor is higher than that of the sample in 6.1. This indicates a higher device sensitivity.

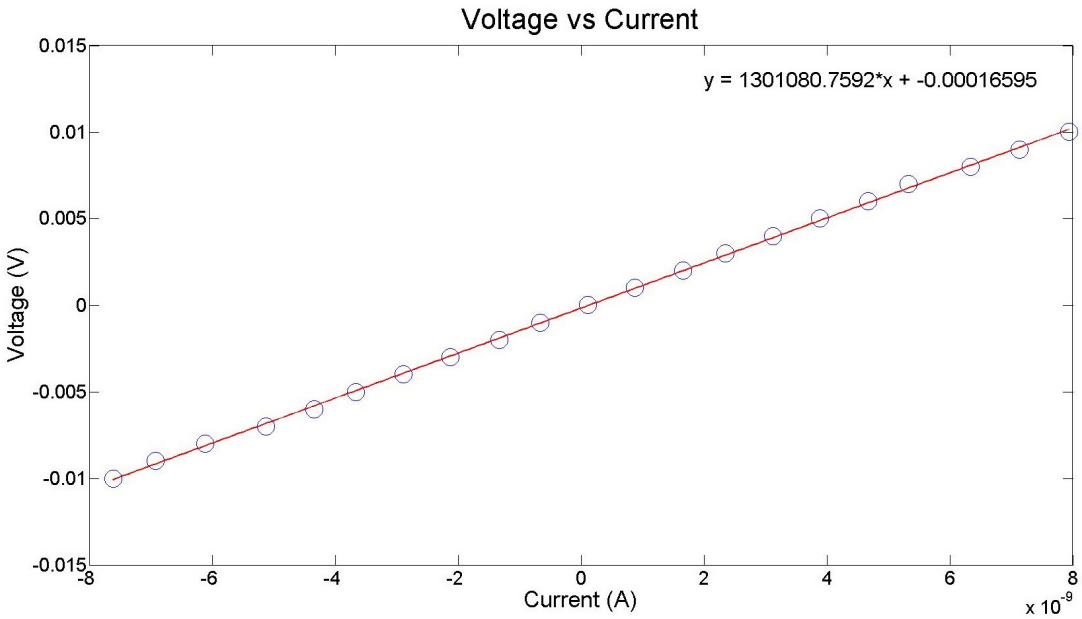

Figure 6.3: Voltage vs Current data used to measure the effective sample resistance of the thermistor at room temperature (approximately 20 ℃), R_0. R_0 is the slope of the trend line and is 1.3 MΩ in this thermistor. The power going into the device must be very low as to not burn out the VO_x, so milli Volts and nano Amps were used.

multiple functioning channels on the same array sample. The second recording, which only highlights channel three from a glass substrate array, is purposed for comparing real-time sensitivity to the one predicted from equation 3.4, which used E_a in figure 6.2. TCR was calculated in the following fashion:

$$V_{out} = V_{in}\frac{R_2 + \delta}{R_1 + R_2 + \delta} \tag{6.1}$$

Where δ is the change in resistance from effective R_0 at the V_{out} output with V_{in} input. Given: R_0 as 1.304 MΩ; V_{out} as 80.55 mV and 68.1 mV; V_{in} as 234 mV (Vref); two deltas were calculated. The percent change in delta was then calculated. Dividing by the known total temperature change, in this case 5 ℃ during the test, yields TCR in %/℃. The result was -4.36 %/℃, which is close to the predicted

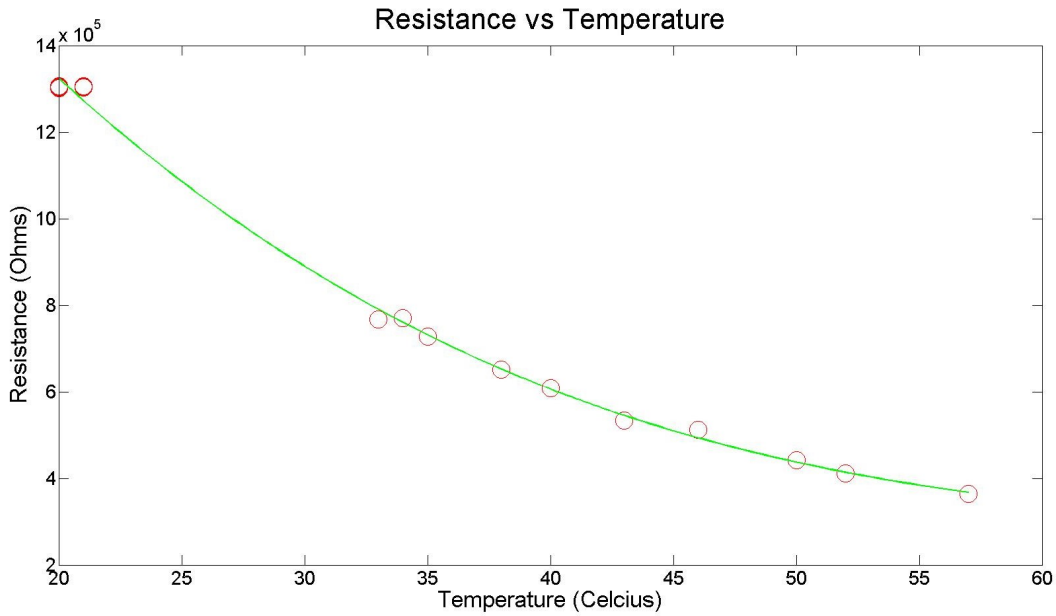

Figure 6.4: Data from the hot plate probe station showing the non-linear relationship of resistance change vs temperature in a thermistor. The trend line is a third-order polyfit.

-4.04 %/℃. The approximate sensitivity in mV/℃ can also be extracted by dividing the voltage change by the total temperature change, yielding 2.5 mV/℃.

Figure 6.7 is the Vref channel used in the recordings. Vref is used by the ADS1299 for differential amplification of the channels. The goal for our sensors is to measure very small temperature gradients in brain, ideally down to the 5–15 mK scale. The peak-to-peak noise shown in Vref is approxiamtely 30 µV. Dividing the 2.5 mV/℃ sensitivity by the 30 µV P-P noise gives a temperature inaccuracy of about 12 mK.

6.3 Thermal Gradient Testing

There are no publishable results at this time for the thermal gradient testing of our arrays. Experimentation will commence as soon as a working PI controller is

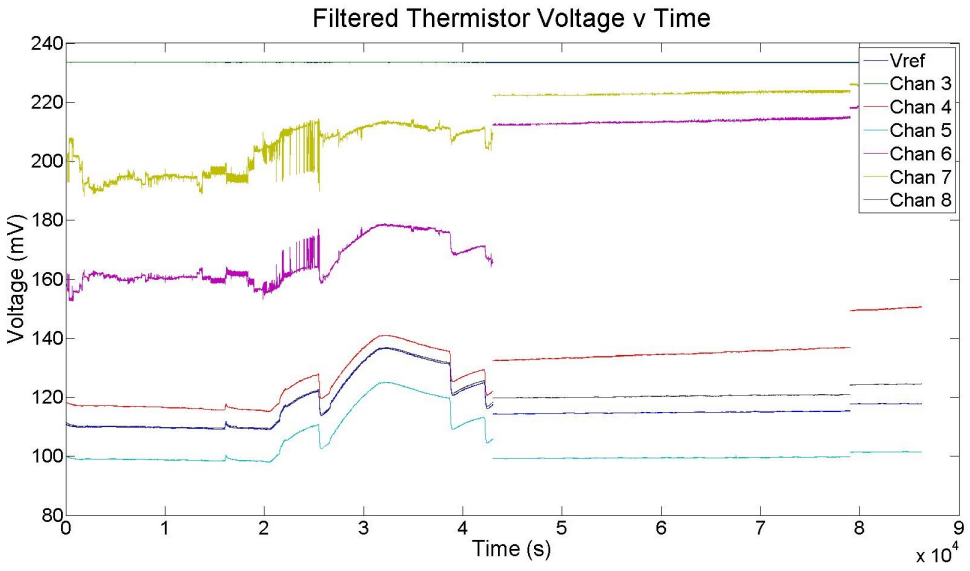

Figure 6.5: Recordings from seven channels taken over the time span of three days. This was done to show temperature tracking from all thermistors in the array. R_0 is different between each thermistor. Channels 6 and 7 (towards the top) have higher levels of noise than the other channels, most likely due to their smaller effective resistances. The thermistors were not passivated and show small resistance drifts over the time course of recording. Vref (top line) is 234 mV.

designed in LabView. This is expected to be within the same month as submission of this thesis.

6.4 Immersion Testing

Immersion testing was performed with a passivated polyimide substrate array. Two working channels from the device were recorded. Results in figure 6.8 show that the array was able to continuously measure temperature change in a liquid ionic environment.

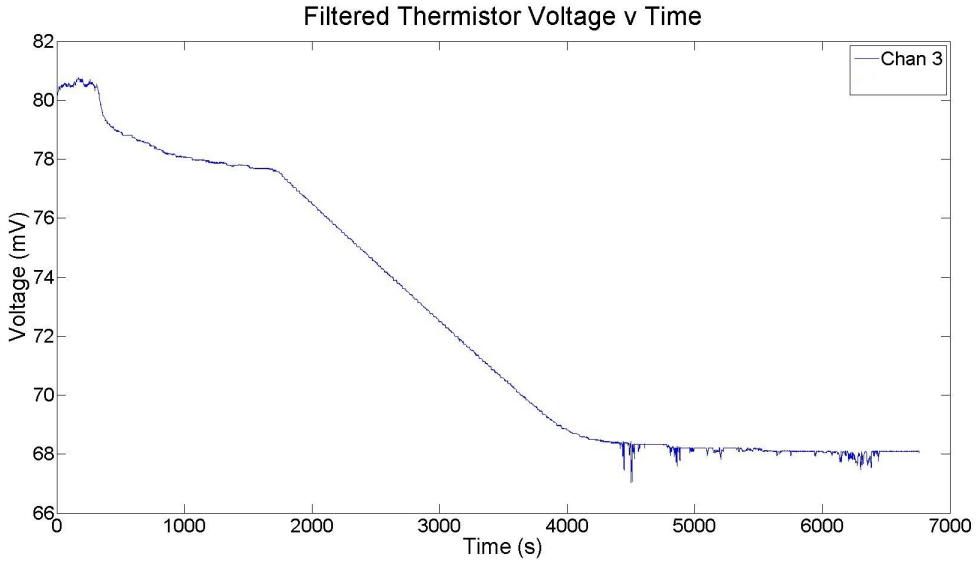

Figure 6.6: A single channel recording from a glass substrate array showing resistance change with a 5 ℃ increase (30 ℃ to 35 ℃) in temperature. Real-time TCR was calculated as -4.30 %/℃. Sensitivity is approximately 2.5 mV/℃ based on this graph.

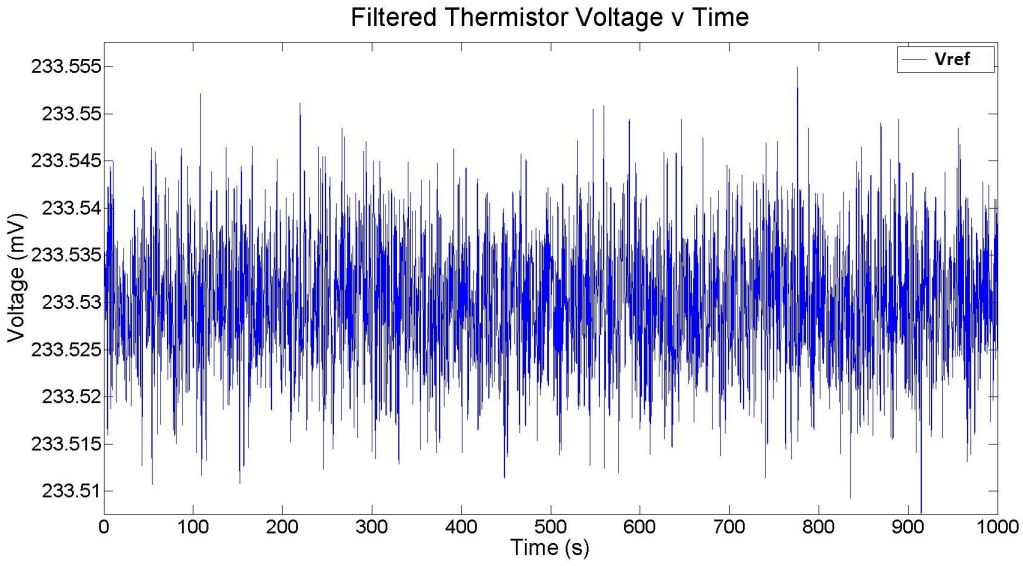

Figure 6.7: Noise from Vref during the recording done in figure 6.6. From peak to peak is approximately 30 µV. This equates to roughly 12 mK of temperature inaccuracy in the recording system.

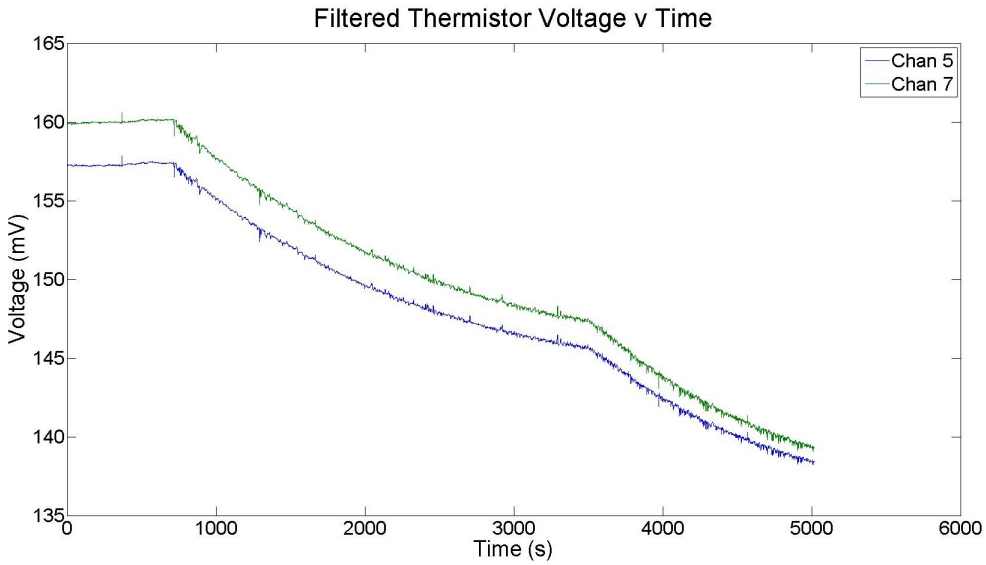

Figure 6.8: Data of a passivated polyimide substrate submerged in saline solution. Continuous temperature changes from 26 ℃ to 35 ℃ to 41 ℃ were measured over the time course of about 80 minutes.

6.5 Array Implantation

Implantation tests of small strips of PEG encapsulated polyimide substrate assisted by silicon shuttles were performed. The results are shown in figures 6.10–6.14. Many of the trials resulted in excess PEG on the implant or shuttle fracture. A successful trial with a full length shuttle was achieved, though the PEG encapsulation could have been thinner and smoother. Results from this experiment show buckling of flexible substrate upon insertion into mechanically brain-like agarose gel (figure 6.9) can be overcome through the use of an encapsulation shell and an implant shuttle. The shuttle can also help improve accuracy in positioning of the implant.

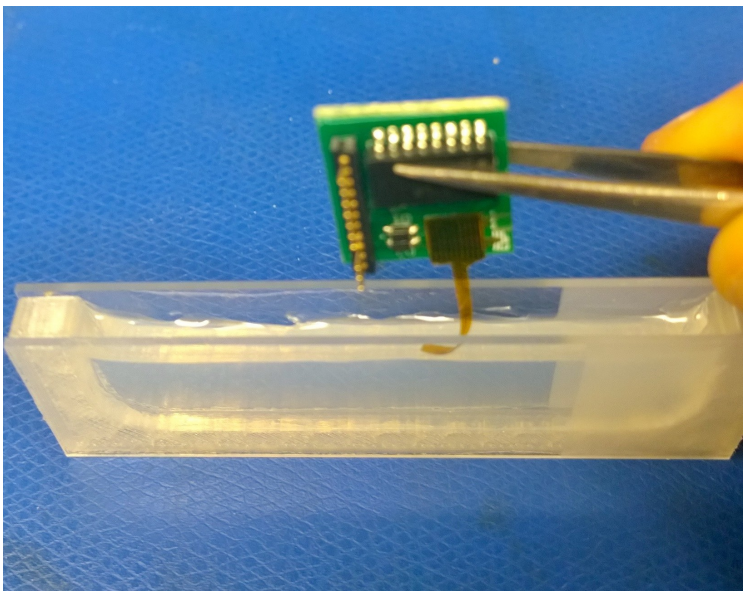

Figure 6.9: Array with polyimide substrate buckling from the force of the agar gel.

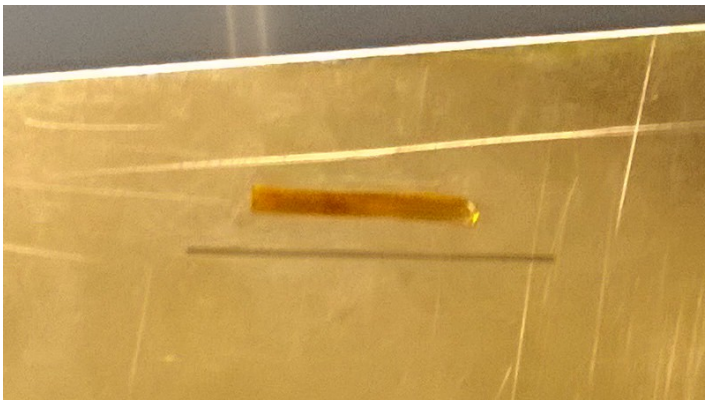

Figure 6.10: Implant next to full Si shuttle. The implant is the full length of the invasive part of the array design, though it is wider than what an in-vivo implant would be.

Figure 6.11: Shuttle and array encapsulated together in PEG. The encapsulation coating is too rough and thick, but still good for demonstration of our design and procedure. The array here is just a polyimide substrate cut out, not the one shown in figure 6.10.

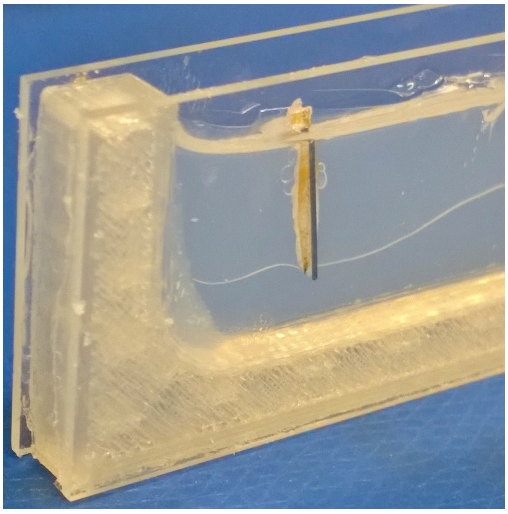

(a) Shuttle and substrate immediately after insertion into the gel. The PEG shell is still there, but dissolved within the minute following the capture of this image.

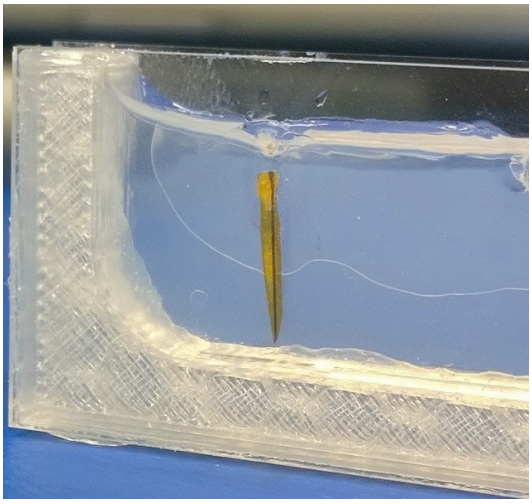

(b) Array with the Si shuttle removed.

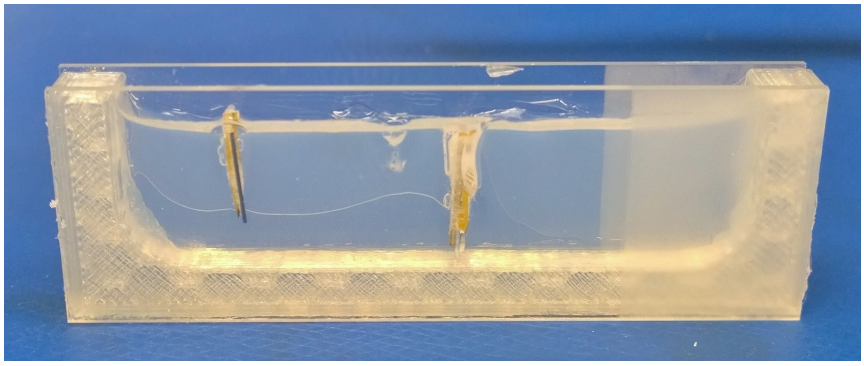

Figure 6.13: Comparison of a good implantation vs a poor one. The PEG shell on the right implant is too large and creates a lot of damage to the surrounding agar gel, whereas the left implant was placed into position without disrupting local gel.

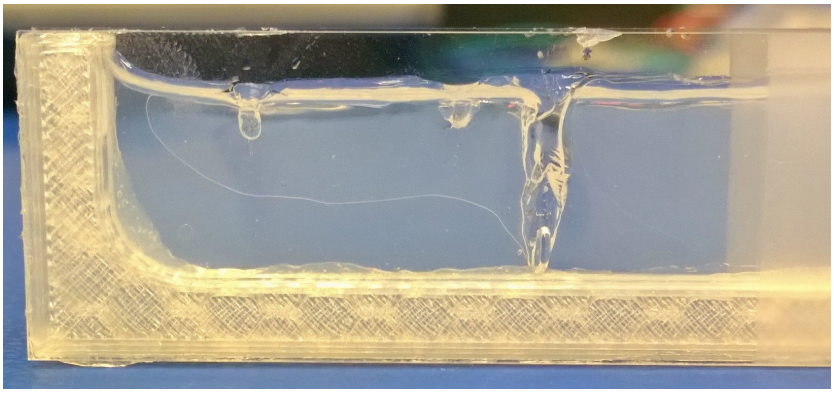

Figure 6.14: The result after both implants from figure 6.13 were removed. The right implant created catastrophic damage to the local agar gel; the left implant left much of the agar intact. The small amount of gel disruption on the left side was caused by the pair of tweezers during Si shuttle retrieval.

Chapter 7
Analysis and Applications

Our eight channel VO_x thermistor array has been presented and tested. Grounded in a background of brain temperature and temperature sensors, the unique design of our device is purposed as a minimally-invasive, highly localized, and very sensitive neural implant. Various experiments were used to characterize sensors and establish the abilities of the complete system. This chapter brings everything together in an analysis of the performance of our arrays and a discussion of its potential for future research and medical applications. Recommendations for improving the design and performing additional tests to further prove the robustness and viability of our system as a neural implant are given where appropriate.

7.1 Discussion and Recommendations

7.1.1 Sample TCR

Real-time sensitivity was calculated to be about -4.3 %/℃ in a glass substrate thermistor sample. This was close to the predicted TCR value of -4.04 %/℃. The difference in sensitivities can be attributed to the data points used as well

as the way in which the real time value was calculated. The only reference for stabilized temperature was the indicator on the heating block; there was no separate temperature measurement taken to use as a reference. The data points used in the calculation were assumed to be from stabilized temperatures of 30 ℃ and 35 ℃. The heating block, however, over heats and over cools around its set point, so the difference in temperature was most likely not exactly 5 ℃.

Furthermore, the data was taken from one channel, as most of the others were not working well. TCR will vary from deposition sample to sample, but the thermistors for any given deposition should have the same sensitivity. Sensitivity from multiple channels should have been calculated. Finally, 5 ℃ is a large domain for performing this type of calculation, and is more representative of the average thermistor sensitivity as opposed to dR/dT. Having a system where very frequently sampled changes in resistance can be monitored with respect to smaller temperature changes would be the most accurate way of measuring real-time sensitivity. This is part of what the heating bridge circuit aims to do.

7.1.2 Acquisition Circuitry

7.1.2.1 Interface Electronics Redesign

The voltage regulation board needs to be redesigned with a correct ADG823 chip footprint, as I made it incorrectly in Eagle. This, along with inputting data commands from the MSP430 to the board, will allow the local ground, H+, to be used to calibrate the thermistors and derive their measurement time constants. Calculations for power dissipation in the Ti wire and heat conduction in the local area to the active VO_x will be used as a predictive guideline for the calibration experiments. If the local heating works, testing of functional channels in the array

would be done much more quickly and accurately compared to the bulk heat testing that was done for this project.

7.1.2.2 Heating Bridge

The heating bridge circuit was fabricated, and in initial, unpublished, testing showed ability to measure room temperature using the TMP37 and dissipate varied levels of power across the transistor and resistor by changing V_b via the Ni-DAQ 6211. This is an essential step in having a stabilized temperature gradient across the FR4, as only the PI code needs to be written to control the power flux between both sides of the board. Once code for the PI controller is written, experimentation will begin immediately.A predictive model of 1-D temperature conduction across the FR4 will also be developed for this experiment to see how our device data compares to equation 5.1. Though testing of small temperature gradient with a fabricated polyimide array will be difficult, due to the lack of working channels on the majority of samples. More devices will be fabricated in the coming months as I continue this project into graduate school.

7.1.3 Immersion Test

Passivated polyimide substrate samples showed successful recording capabilities while immersed in a liquid ionic environment. There did, however, seem to be a little more noise in the working channels than there were in recordings performed during other tests. This could be attributed to either the submergence in saline, a decrease in resistance over the several months from when the samples were deposited to when they were tested, or the use of polyimide substrate samples over the glass ones. Dr. Basantani made these sample depositions only a day before leaving Penn

State. This situation gave little time to thoroughly examine the deposition quality. Many of the channels from the polyimide samples had significant noise and were not working outside of the immersion test. Poor sample quality may have played a big role in the results from this test. Images of poor fabrication, where metal deposits or particles are shorting channels, can be seen in figures 7.1 and 7.2.

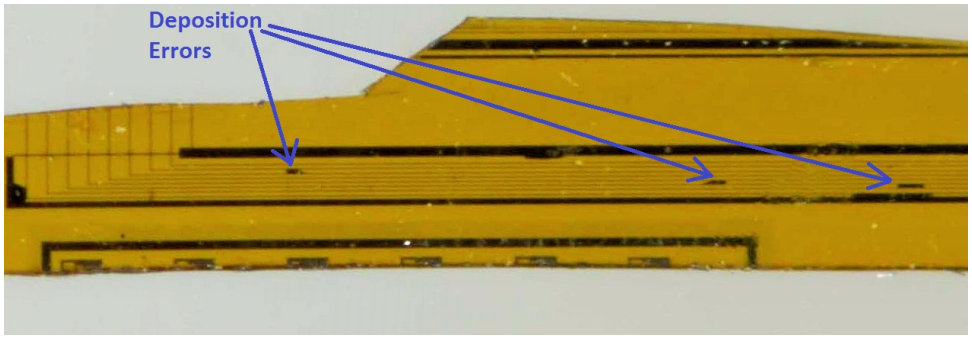

Figure 7.1: Polyimide substrate deposition with Ti deposits shorting leads together, resulting in broken channels.

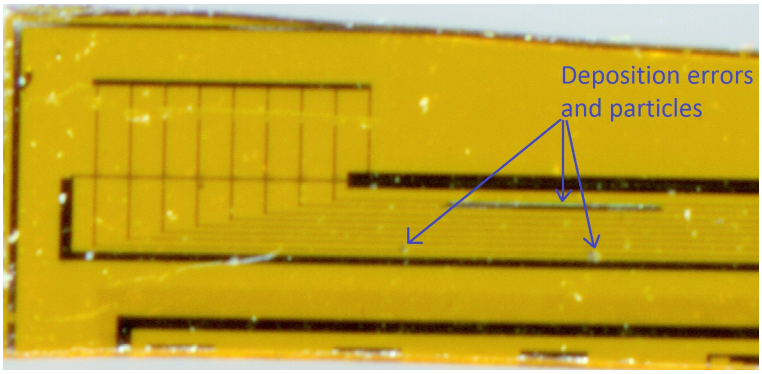

Figure 7.2: Another polyimide substrate deposition showing metal deposit shorts and extraneous particles on the channel leads. This sample was the one used in immersion testing.

Additionally, the test was performed using inexact temperature set points because the hot plate used was not very accurate. A more robust data set would have been one where exact temperature set points were reached and changes were made in periodic intervals. The immersion test done for this project accomplished

its goal of showing functionality of our devices in a brain-like liquid environment though. In the future, passivated arrays with many functioning channels should be tested while submerged in saline form multiple days to show chronic recording capabilities. Imaging of pre and post chronic immersion testing samples should also be taken to observe any delamination of the parylene or corrosion of the device.

7.1.4 Implantation Procedure

The implantation of an encapsulated array supported by a silicon shuttle was successful, but there were many failed trails during the experiment. The main issue was cleavage of the Si shuttles. Fracture occurred at a 45° angle because of the (1 1 1) Miller indices of the wafer used for dicing. This type of silicon seems to be unsuited for bearing the shear stresses created from probe insertion. The overall length of the shuttle should be shorter too. Buckling is more likely to occur in longer columns, but a shorter shuttle would be okay for *in-vivo* implantation.

The PEG encapsulation was rough and too thick, though not too much so that the results of the experiments were undermined. A slower dip in a larger, more filled container of PEG, either by hand or by a motorized device, would help smooth out and thin the shell. A technique for dipping the array and shuttle simultaneously so that they are as closely fit and narrow together as possible needs to be examined in the future. This would improve the accuracy of the implant placement as well as reduce the overall disruption of local brain tissue.

7.2 Future Goals

Our VO_x thermistor array has the potential to be a great tool for future neuro-scientific and biomedical research, and as a medical device to help improve people's

lives. While this project only took a first look at the device and its characteristics, the results show promise for the array moving past these initial design stages and into more specific research and engineering applications. I will be continuing research on this project as I pursue an M.S degree through the Engineering Science and Mechanics integrated undergraduate-graduate (IUG) program. The goals laid out in the following section are part of what I hope to accomplish with this project over the next year.

7.2.1 Next Steps and Future Research Applications

The goal for this project over the next year is to perform *in-vivo* recordings in seizure rats. Understanding focal seizures at the spatial and thermal resolution that our device offers could have tremendous implications on the way neuroscientists examine seizure activity. The main steps that need to be taken in order to reach this goal are: redesign aspects of the interface electronics; deposit new samples on polyimide substrate to get all channels working; test an array's ability to measure stabilized temperature fields using a heating bridge circuit; refine the implantation procedure to minimize excess PEG during encapsulation and replace design of the shuttle to reduce catastrophic failures. All of these have been addressed through recommendations in previous sections. Preliminary *in-vivo* experimentation and data analysis is a realistic goal for the next year given the current state of the device design and its abilities.

Visions for future research applications of the thermistor array include adding electrodes to the deposition layout and using the device for temperature sensing in other parts of the body. EEG electrodes are commonly used to monitor neural activity. Placing comparably-sized electrodes next to the temperature sensors could

provide a more comprehensive picture of what is happening in brain on a localized scale when both normal and abnormal physiological changes are occurring. In a different vein, given the biocompatible and flexible nature of our design, the array could be implanted into muscle and blood vessels. It could also be thermally coupled to the surface of organ tissue, such as heart, and measure small temperature gradients there. Hopefully, future collaborations with other research groups who are interested in using our array design to study localized temperature fields in brain and body will be possible.

7.2.2 Early Seizure Detection and Prevention

As mentioned previously, seizure activity is correlated to local temperature changes due to increased blood flow, metabolism, and neuronal cell activity. A very sensitive temperature sensor would be able to detect these physiological changes prior to the onset of full seizure activity. This could be extremely useful if employed as part of a feedback loop mechanism for early seizure detection, one which could warn an epileptic patient to stop what they are doing, get in a safe position, and inform a medical professional if necessary. This could greatly reduce the physical dangers associated with sudden seizure events as well as improve the quality of the patient's social life.

Additionally, early research in induced localized hypothermia as a treatment for epilepsy has shown promise in mitigation and possible prevention of seizure activity [78] [79] [80]. Our thermistor array could measure pre-seizure temperature fluctuations, indicating how soon and how intense an oncoming event will be, and trigger a localized cooling device in attempts to reduce the magnitude of the attack or prevent it all together. Using an array like ours to implement these sorts of

systems could be a great help to the physical and social health of anybody suffering from chronic seizure events.

7.3 Conclusion

Our design for an neural temperature sensor array using novel thin-film, vertically-integrated vanadium oxide thermistors shows great potential for minimally-invasive and highly localized temperature gradient measurements with a spatial and thermal resolution better than most contemporary devices currently being used in neural engineering. While the project is still in its early stages of testing and continued development, key tests have proven the essential concepts of our design. Further improvements must be made to the device. New samples must be fabricated and modifications must be made to the complementary electronics. This could reduce electrical noise and would add additional capabilities to the design. Given success with these tasks, our sensors could offer a low cost, high quality temperature measurement and recording system that can be used for many different research and medical applications. While the main motivation for my efforts was to move closer to improving the quality of life for people with epilepsy, I am excited to also see other outcomes that our device will achieve.

Appendix A
Reference Material

A.1 Rat Brain

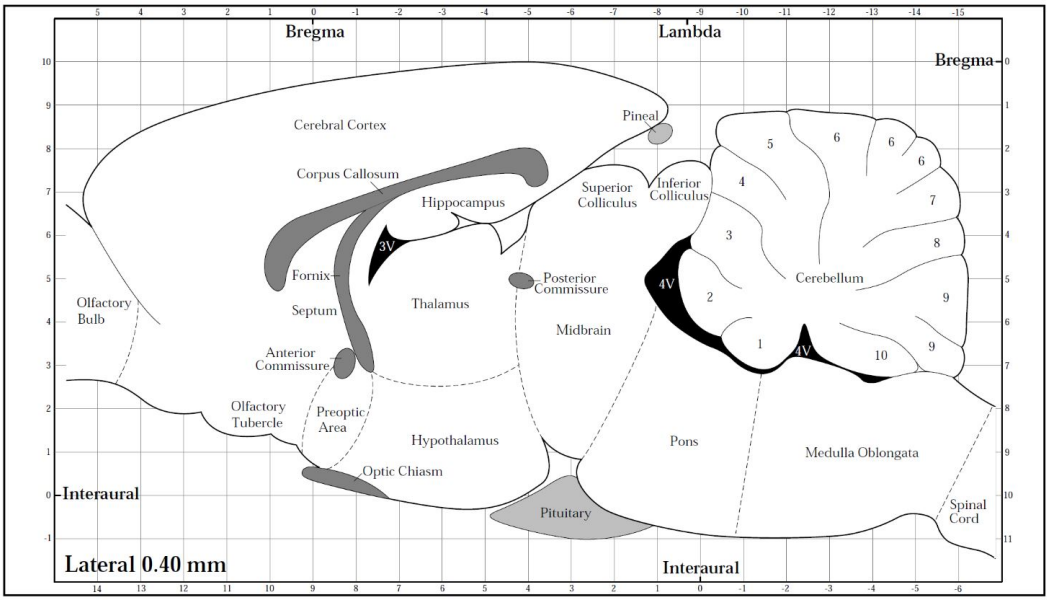

Figure A.1: A stereotaxic map sagittally sectioned rat brain 0.40 mm lateral from Bregma. Hippocampus is about 2.5–4.25 mm in depth. Hypothalmus, which is the temperature regulation region of brain, is about 8–10.25 mm. Taken from Paxinos and Watson [61].

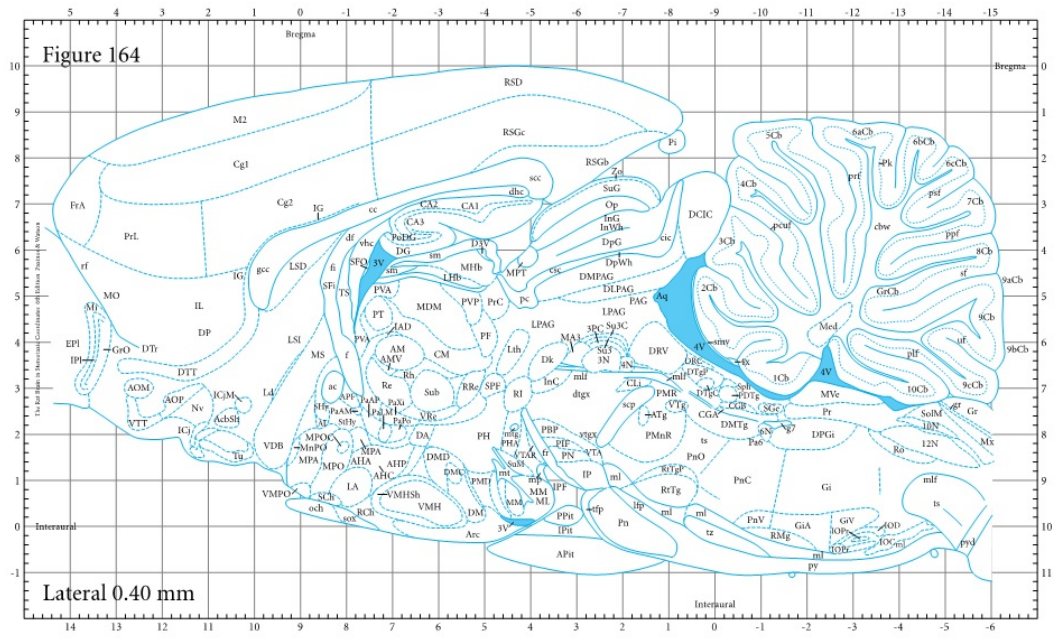

Figure A.2: Another sagital cross-section of rat brain at 0.40 mm lateral from Bregma. The same regions seen in figure A.2 are further differentiated into their respective anatomical subfields [61].

Appendix B
MATLAB Code

B.1 Excel Import and TCR Calculation

```
%Myles Billard
%Thesis Project
%Jan 2015

%%%
%TCR Data analysis from Hot plate probe station
%%%

clear all
close all
clc

%import excel file
file = xlsread('Through Film Single.xlsx',9);

```

```
%assign file column values to different parameters
temp = file(:,6);
res = file(:,8);
KbT_Inverse = file(:,9);
lnRes = file(:,10);

%plot resistance vs temperature --> non-linear result
figure;
plot(temp,res, 'ro','markers',20);
set(gca,'fontsize',22)
xlabel('Temperature (Celcius)', 'fontsize',26)
ylabel('Resistance (Ohms)','fontsize',26)
title('Resistance vs Temperature', 'fontsize', 32);
[coeffs] = polyfit(temp, res, 3);
a = coeffs(1);
b = coeffs(2);
%polyfit_str = ['y = ' num2str(a) '*x + ' num2str(b)];

%%best fit line
fittedTemp = linspace(min(temp), max(temp), 200);
fittedRes = polyval(coeffs, fittedTemp);
hold on;
plot(fittedTemp, fittedRes, 'g-', 'LineWidth', 2);
%text(55,4.5E5,polyfit_str,'fontsize',16);

%%plot ln(res) vs 1/KbT
figure;
```

```
plot(KbT_Inverse, lnRes, 'kd','markers',20);
set(gca,'fontsize',33)
xlabel('1/Kb*T (eV)','fontsize',26);
ylabel('ln(Res)','fontsize',26)
title('ln(Res) vs 1/KbT','fontsize',32);

%%best fit line
[coeffs1] = polyfit(KbT_Inverse, lnRes, 1);
a = coeffs1(1);
b = coeffs1(2);
Ea = a;
TCR = -Ea/(8.6173324E-5*293^2)*100;
polyfit_str = ['y = ' num2str(a) '*x + ' num2str(b)];
fittedKbT_Inverse = linspace(min(KbT_Inverse),...
max(KbT_Inverse), 200);
fittedlnRes = polyval(coeffs1, fittedKbT_Inverse);
hold on;
plot(fittedKbT_Inverse, fittedlnRes, 'r-', 'LineWidth', 2);
text(38.65,13.7,polyfit_str,'fontsize',24);
text(38.65,13.6,['Ea = ' num2str(Ea) 'eV'],'fontsize',24);
text(38.65,13.5,['TCR = ' num2str(TCR) '% / \circK'],...
'fontsize',24);

%%%%%%%%%%%%%%%%%%%%%%%%%%%%%%%%%%%%%%%%%%%%%%%%%%%%%%%%%%%%%%%%%%%%%%%
%Now reading current vs voltage for TCR test
%follows same procedure as above code
%for importing and plotting
```

```
70
file = xlsread('Through Film Single.xlsx',2);
Voltage = file(:,1);
Current = file(:,2);

75 %plotting data
figure;
plot(Current, Voltage, 'bo','markers',20);
set(gca,'fontsize',22)
xlabel('Current (A)','fontsize',26)
80 ylabel('Voltage (V)','fontsize',26)
title('Voltage vs Current','fontsize',32);
[coeffs] = polyfit(Current, Voltage, 1);
a = coeffs(1);
b = coeffs(2);
85 polyfit_str = ['y = ' num2str(a) '*x + ' num2str(b)];

%%best fit line
fittedI = linspace(min(Current), max(Current), 200);
fittedV = polyval(coeffs, fittedI);
90 hold on;
plot(fittedI, fittedV, 'r-', 'LineWidth', 2);
text(2E-9,.013,polyfit_str,'fontsize',24);
```

B.2 Channel File Read and Plot

```
%Credit: Dr. Madineh Sedigh-Sarvestani
%for the read file section of this code

clc
clear all
close all

%-------------------------------------------------------
%Read .bin file

%% first setup the path where the .bin files are stored
pfn= 'C:\Users\Example

D = dir([pfn '\*.bin']);



mRC1=2;mRC2 = 9; SPl1=3; SPl2=6; %check order in header

tlast_old = 0;

for l=1:length(D)%[10:length(d)] %file range of interest

    s.fn = [pfn D(l).name];
    h = read_hdr1(s.fn);
    sf=h.sample_rate;
    s.nsec=h.total_file_length;
```

```
    s.chan =(2:9);
    vref = 234;

   [x,t]=read_daq_file_MSP(s);

%-------------------------------------------------------
%removing the offset caused by ref > pos differential input
x = x(:,:)+vref;

%Butterworth stopband filter, taking out 60Hz noise
[nn,wn]=buttord([55 65]/(sf/2),[59 61]/(sf/2),3,5);
[c, d]=butter(nn,wn,'stop');

xx=filtfilt(c,d,x);

%Low PAss freq=6Hz here
[b_lp,a_lp]=butter(6,1/(sf/2),'low');

xx = filtfilt(b_lp,a_lp,xx);

%plotting

plot(t+tlast_old,xx(:,:));
set(gca,'fontsize',24);
hold on

ylabel('Voltage (mV)','fontsize',28)
```

```
xlabel('Time (s)','fontsize',28)
title('Filtered Thermistor Voltage v Time','fontsize',32)
legend('Vref','Chan 3','Chan 4','Chan 5',...
'Chan 6','Chan 7','Chan 8')


tlast_old = tlast_old + max(t);
end
```

Bibliography

[1] Benke, T. A. and J. Swann (2004) "The Tetanus Toxin Model of Chronic Epilepsy," in *Recent advances in epilepsy research* (D. K. Binder and H. E. Scharfman, eds.), chap. 16, Springer, pp. 226–238.

[2] Rango, M., A. Arighi, and N. Bresolin (2012) "Brain temperature," *NeuroReport*, **23**, pp. 483–487.

[3] Kiyatkin, E. a. (2010) "Brain temperature homeostasis: physiological fluctuations and pathological shifts." *Frontiers in bioscience : a journal and virtual library*, **15**(443), pp. 73–92.

[4] Mellergå rd, P. (1995) "Intracerebral temperature in neurosurgical patients: intracerebral temperature gradients and relationships to consciousness level." *Surgical neurology*, **43**(94), pp. 91–95.

[5] Schmidt-Nielsen, K. (1997) *Animal physiology: adaptation and environment*, Cambridge University Press.

[6] (1979) "Brain energy metabolism by B. K. Siesjo, John Wiley & Sons, New York, 1978," *Annals of Neurology*, **5**(3), p. 308.
URL `http://dx.doi.org/10.1002/ana.410050318`

[7] Jensen, FrankB. and Weber, R. (1987) "No Title," *Journal of Comparative Physiology B*, **157**, pp. 137–143.

[8] Gerasimov, V. (1998) "Information processing in human body," .
URL `WWWhttp://www.vadim.www.media.mit.edu/MAS862/Project.html`

[9] Yablonskiy, D. a., J. J. Ackerman, and M. E. Raichle (2000) "Coupling between changes in human brain temperature and oxidative metabolism during prolonged visual stimulation." *Proceedings of the National Academy of Sciences of the United States of America*, **97**(13), pp. 7603–7608.

[10] Kiyatkin, E. a., P. L. Brown, and R. a. Wise (2002) "Brain temperature fluctuation: A reflection of functional neural activation," *European Journal of Neuroscience*, **16**(April), pp. 164–168.

[11] Dittmar, a., C. Gehin, G. Delhomme, D. Boivin, G. Dumont, and C. Mott (2006) "A non invasive wearable sensor for the measurement of brain temperature." *Conference proceedings : ... Annual International Conference of the IEEE Engineering in Medicine and Biology Society. IEEE Engineering in Medicine and Biology Society. Conference*, **1**, pp. 900–902.

[12] Walker, M. P. and R. Stickgold (2014) "Sleep, memory and plasticity," *Neuroscience and Psychoanalysis*, **1**, p. 93.

[13] Buzsáki, G. (2002) "Theta oscillations in the hippocampus," *Neuron*, **33**(3), pp. 325–340.

[14] Ermis, U., K. Krakow, and U. Voss (2010) "Arousal thresholds during human tonic and phasic REM sleep: Phasic and tonic REM sleep," *Journal of Sleep Research*, **19**, pp. 400–406.

[15] Parmeggiani, P. (2007) "Brain Temperature in REM Sleep," *Archives Italiennes de Biologie*, **145**, pp. 13–21.

[16] Schiff, S. J. and G. G. Somjen (1985) "The effects of temperature on synaptic transmission in hippocampal tissue slices." *Brain research*, **345**(2), pp. 279–284.

[17] Andersen, P. and E. I. Moser (1995) "Brain temperature and hippocampal function," *Hippocampus*, **5**(6), pp. 491–498.
URL `http://dx.doi.org/10.1002/hipo.450050602`

[18] Kim, J. a. and B. W. Connors (2012) "High temperatures alter physiological properties of pyramidal cells and inhibitory interneurons in hippocampus," *Frontiers in Cellular Neuroscience*, **6**(July), pp. 1–12.

[19] Yang, X. F., J. H. Chang, and S. M. Rothman (2002) "Intracerebral temperature alterations associated with focal seizures," *Epilepsy Research*, **52**, pp. 97–105.

[20] NIH (2014) "Seizures and Epilepsy: Hope through Research," .
URL `http://www.ninds.nih.gov/disorders/epilepsy/detail\_epilepsy`

[21] Dymond, A. M. and P. H. Crandall (1973) "Intracerebral temperature changes in patients during spontaneous epileptic seizures," *Brain Research*, **60**, pp. 249–254.

[22] Dymond, a. M. and P. H. Crandall (1976) "Oxygen availability and blood flow in the temporal lobes during spontaneous epileptic seizures in man," *Brain Research*, **102**, pp. 191–196.

[23] Rossi, S., E. R. Zanier, I. Mauri, a. Columbo, and N. Stocchetti (2001) "Brain temperature, body core temperature, and intracranial pressure in acute cerebral damage." *Journal of neurology, neurosurgery, and psychiatry*, **71**, pp. 448–454.

[24] Melville, I. (1987) *Recent Advances in Epilepsy. No. 3*, vol. 63.

[25] Lowenstein, D. H. (2005) "Seizures and epilepsy," *Harrisons principles of internal medicine*, **16**(2), p. 2357.

[26] Rumana, C. S., S. P. Gopinath, M. Uzura, a. B. Valadka, and C. S. Robertson (1998) "Brain temperature exceeds systemic temperature in head-injured patients." *Critical care medicine*, **26**, pp. 562–567.

[27] Schwab, S., M. Spranger, a. Aschoff, T. Steiner, and W. Hacke (1997) "Brain temperature monitoring and modulation in patients with severe MCA infarction." *Neurology*, **48**, pp. 762–767.

[28] Dietrich, W. D., R. Busto, M. Halley, and I. Valdes (1990), "The importance of brain temperature in alterations of the blood-brain barrier following cerebral ischemia." .

[29] Busto, R., W. D. Dietrich, M. Y. Globus, I. Valdés, P. Scheinberg, and M. D. Ginsberg (1987) "Small differences in intraischemic brain temperature critically determine the extent of ischemic neuronal injury." *Journal of cerebral blood flow and metabolism : official journal of the International Society of Cerebral Blood Flow and Metabolism*, **7**, pp. 729–738.

[30] Martinit, F. H., J. L. Nath, and E. F. Bartholomew (2012) *Fundamentals of Anatomy & Physiology*, 9th ed., Pearson.

[31] Miller, K., K. Chinzei, G. Orssengo, and P. Bednarz (2000) "Mechanical properties of brain tissue in-vivo: Experiment and computer simulation," *Journal of Biomechanics*, **33**, pp. 1369–1376.

[32] Sridharan, A., S. D. Rajan, and J. Muthuswamy (2013) "Long-term changes in the material properties of brain tissue at the implant-tissue interface." *Journal of neural engineering*, **10**, p. 066001.
URL `http://www.ncbi.nlm.nih.gov/pubmed/24099854`

[33] Polikov, V. S., P. a. Tresco, and W. M. Reichert (2005) "Response of brain tissue to chronically implanted neural electrodes," *Journal of Neuroscience Methods*, **148**, pp. 1–18.

[34] Lee, H., R. V. Bellamkonda, W. Sun, and M. E. Levenston (2005) "Biomechanical analysis of silicon microelectrode-induced strain in the brain." *Journal of neural engineering*, **2**, pp. 81–89.

[35] Wester, B. a., R. H. Lee, and M. C. LaPlaca (2009) "Development and characterization of in vivo flexible electrodes compatible with large tissue displacements." *Journal of neural engineering*, **6**, p. 024002.

[36] Richardson, R. R., J. a. Miller, and W. M. Reichert (1993) "Polyimides as biomaterials: Preliminary biocompatibility testing," *Biomaterials*, **14**(8), pp. 627–635.

[37] Kim, J., T. J. Richner, S. Thongpang, K. a. Sillay, D. B. Niemann, A. S. Ahmed, L. a. Krugner-Higby, and J. C. Williams (2009) "Flexible thin film electrode arrays for minimally-invasive neurological monitoring," *Proceedings of the 31st Annual International Conference of the IEEE Engineering in Medicine and Biology Society: Engineering the Future of Biomedicine, EMBC 2009*, pp. 5506–5509.

[38] Lee, K.-k., J. He, A. Singh, S. Massia, G. Ehteshami, B. Kim, and G. Raupp (2004) "Polyimide-based intracortical neural implant with improved structural stiffness," *Journal of Micromechics and Microengineering*, **32**, pp. 32–37.

[39] Rousche, P. J., D. S. Pellinen, D. P. Pivin, J. C. Williams, R. J. Vetter, and D. R. Kipke (2001) "Flexible polyimide-based intracortical electrode arrays with bioactive capability," *IEEE Transactions on Biomedical Engineering*, **48**(3), pp. 361–370.

[40] Takeuchi, S., Y. Yoshida, D. Ziegler, K. Mabuchi, and T. Suzuki "Parylene Flexible Neural Probe," , pp. 208–211.

[41] Lago, N., K. Yoshida, K. P. Koch, and X. Navarro (2007) "Assessment of biocompatibility of chronically implanted polyimide and platinum intrafascicular electrodes," *IEEE Transactions on Biomedical Engineering*, **54**(2), pp. 281–290.

[42] Laursen, H. and N. H. Diemer (1980) "Capillary size, density and ultrastructure in brain of rats with urease-induced hyperammonaemia." *Acta neurologica Scandinavica*, **62**, pp. 103–115.

[43] Schlageter, K. E., P. Molnar, G. D. Lapin, and D. R. Groothuis (1999) "Microvessel organization and structure in experimental brain tumors: microvessel populations with distinctive structural and functional properties." *Microvascular research*, **58**, pp. 312–328.

[44] Schmidt, E. M., J. S. Mcintosh, and M. J. Bak (1988) "Long-term implants of Parylene-C coated microelectrodes," *Medical & Biological Engineering and Computing*, **26**, pp. 96–101.

[45] Hench, L. L., A. R. Boccaccini, R. M. Day, and S. M. Gabe (2003) "Third-Generation Gene-Activating Biomaterials," *Materials Science Forum*, pp. 426 – 432.

[46] Horowitz, P. and W. Hill (1989) "The Art of Electronics," in *The Art of Electronics*, 2nd ed., chap. 15, Cambridge University Press, pp. 988–993.

[47] Feteira, A. (2009) "Negative temperature coefficient resistance (NTCR) ceramic thermistors: An industrial perspective," *Journal of the American Ceramic Society*, **92**, pp. 967–983.

[48] Lyons, B. E., T. V. Samulski, and R. H. Britt (1985) "Temperature Measurements in High Thermal Gradients: I. The Effects of Conduction," *International journal of radiation oncology, biology, physics*, **34686**(December 1984).

[49] Lee, B. C., Y. Lim, K. Kim, S. Lee, and S. Moon (2009) "MICROFABRICATED NEURAL THERMOCOUPLE ARRAYS PROBE FOR BRAIN RESEARCH Nano-Bio Research Center , KIST , Seoul , KOREA Center for Neural Science , KIST , Seoul , KOREA Memory Division , Samsung Electronics Co ., Ltd ., Gyeonggi-do , KOREA ABSTRACT," *Measurement*, pp. 338–341.

[50] "RTD, Thermocouple, or Thermistor?" , p. 10.

[51] Li, C., P. M. Wu, Z. Wu, C. H. Ahn, D. Ledoux, L. a. Shutter, J. a. Hartings, and R. K. Narayan (2012) "Brain temperature measurement: A study of in vitro accuracy and stability of smart catheter temperature sensors," *Biomedical Microdevices*, **14**, pp. 109–118.

[52] Fraden, J. (1996) *Handbook of Modern Sensors*, 2nd ed., Springer-Verlag, Baltimore, MD.

[53] Basantani, H. a. (2014) *Thin Film Materials and Devices for Resistive Temperature Sensing Applications*, Phd, The Pennsylvania State University.

[54] Basantani, H. a., H.-B. Shin, T. N. Jackson, and M. W. Horn (2013) "Vertically integrated pixel microbolometers for IR imaging using high-resistivity VOx," **8704**, pp. 87041A–87041A–5.

[55] Jin, Y., H. a. Basantani, A. Ozcelik, T. N. Jackson, and M. W. Horn (2013) "High-resistivity and high-TCR vanadium oxide thin films for infrared imaging prepared by bias target ion-beam deposition," **8704**, p. 87043C.
URL `\url{http://proceedings.spiedigitallibrary.org/proceeding.aspx?doi=10.1117/12.2016277}`

[56] Doras, A. (2013) *DESIGN , CHARACTERIZATION , AND APPLICATION OF INTRACRANIAL TEMPERATURE SENSORS UTILIZING ZINC OXIDE THIN-FILM TRANSISTORS*, Undergraduate honors, The Pennsylvania State University.

[57] Kim, I., H. H. R. Fok, Y. Li, T. N. Jackson, and B. J. Gluckman (2011) "Polymer substrate temperature sensor array for brain interfaces," *2011 Annual International Conference of the IEEE Engineering in Medicine and Biology Society*, pp. 3286–3289.

[58] Corbett, R., a. Laptook, and P. Weatherall (1997) "Noninvasive measurements of human brain temperature using volume-localized proton magnetic resonance spectroscopy." *Journal of cerebral blood flow and metabolism : official journal of the International Society of Cerebral Blood Flow and Metabolism*, **17**, pp. 363–369.

[59] Hollis, V., T. Binzoni, and D. Delpy (2001) "Non Invasive Monitoring of Brain Tissue Temperature by Near-infrared Spectroscopy," **4250**, pp. 470–481. URL `http://discovery.ucl.ac.uk/187706/`

[60] Maruyma, K., S. Mizushina, T. Sugiura, G. V. Leeuwen, J. Hand, G. Marrocco, F. Bardati, a.D. Edwards, D. Azzopardi, and D. Land (2000) "Feasibility of noninvasive measurement of deep brain temperature in newborn infants by multifrequency microwave radiometry," *IEEE Transactions on Microwave Theory and Techniques*, **48**(11), pp. 2141–2147.

[61] Herman, J. P. and S. J. Watson (1987) "The rat brain in stereotaxic coordinates (3nd edn)," *Trends in Neurosciences*, **10**(10), p. 439.

[62] Wortman, J. J. and R. A. Evans (1965) "Young's modulus, shear modulus, and Poisson's ratio in silicon and germanium," *Journal of applied physics*, **36**(1), pp. 153–156.

[63] Takeuchi, S., T. Suzuki, K. Mabuchi, and H. Fujita (2003) "3D flexible multichannel probe array," *The Sixteenth Annual International Conference on Micro Electro Mechanical Systems, 2003. MEMS-03 Kyoto. IEEE*, **14**, pp. 104–107.

[64] Stieglitz, T., S. Member, M. Schuettler, B. Rubehn, S. Member, J. Badia, and X. Navarro (2011) "Evaluation of Polyimide As Substrate Material for Electrodes to Interface the Peripheral Nervous System," *Proceedings of the 5th International IEEE EMBS Conference on Neural Engineering*, pp. 529–533.

[65] Systems, S. C. (2007), "SCS Parylene Dimer," .

[66] Li, L. and A. J. Mason (2010) "Post-CMOS parylene packaging for on-chip biosensor arrays," *Proceedings of IEEE Sensors*, pp. 1613–1616.

[67] Tan, C. P. and H. G. Craighead (2010) "Surface engineering and patterning using parylene for biological applications," *Materials*, **3**(3), pp. 1803–1832.

[68] Gorham, W. F. (1966) "Synthetic Method for," *Journal of Polymer Science*, **4**, pp. 3027–3039.

[69] Nabi, A., I. Kim, A. Alexander, B. Shanmugasundaram, S. J. Schiff, and J. Bruce (2014) "Low Cost Multi Purpose Biopotential Recording System," .

[70] Instruments, T. (2011), "TLV712xx 300-mA , Sub-Bandgap Output Voltage , Low-I Q , Low-Dropout Regulator TLV712xx," .

[71] Inc, A. (2002), "CMOS Low Voltage 1 âĎę Dual SPST Switches Preliminary Technical Data ADG821/ADG822/ADG823," .

[72] Dale, V. (2014), "Wirewound Resistors, Precision Power, Surface Mount," .

[73] Instruments, T. (2013), "Low Voltage Temperature Sensors," .

[74] Mide Technology (2011), "Volture Products - Material Properties," .
URL `http://www.mide.com/pdfs/volture\_material\_properties\_2010`

[75] Burak, J. L. and J. A. Todd (2011) *No Title*, Ph.D. thesis, The Pennsylvania State University.

[76] Dawe, B. and R. Erickson (2008) "Convection-enhanced delivery into agarose gel brain tissue phantoms," *The Journal of Young Investigators*, **18**.

[77] Aldrich, S. (1996), "Agarose," .
URL `http://www.sigmaaldrich.com`

[78] Rothman, S. and X.-F. Yang (2003) "Local Cooling: A Therapy for Intractable Neocortical Epilepsy," *Epilepsy Currents*, **3**(5), pp. 153–156.

[79] Motamedi, G. K., R. P. Lesser, and S. Vicini (2013) "Therapeutic brain hypothermia, its mechanisms of action, and its prospects as a treatment for epilepsy," *Epilepsia*, **54**(6), pp. 959–970.

[80] Osorio, I., G. Kochemasov, V. Baranov, V. Eroshenko, T. Lyubynskaya, and N. Gopalsami (2007) "Implantable brain microcooler for the closed-loop system of epileptic seizure prevention," , pp. 911–914.

Myles Billard

529 Shore Dr., New Windsor, NY 12553 | 845-248-4872 | myles.billard@gmail.com | mylesbillard.com

Education:

The Pennsylvania State University, University Park, PA May 2015

- B.S. in Engineering Science
- Minor: Biomedical Engineering
- Thesis Title: *Localized Temperature Field Measurements of Brain via thin-film Vanadium Oxide Sensor Arrays on Flexible Substrate*
- *Schreyer Honors College* – Top 5% of PSU undergraduates; requires separate admissions process

Related Experience:

Research Assistant Feb. 2012 – Present

Penn State Center for Neural Engineering: Dr. Gluckman Seizure Group

- Develop and debug EEG and temperature acquisition systems using Eagle PCB, SolidWorks, and circuit design skills
- Work with multi-disciplinary engineering teams to converge upon better solutions for recording seizure activity in brain
- Analyze EEG data with NI Labview and MATLAB to generate comprehensive seizure statistics and analysis
- Critically review recent papers related to Epilepsy and other research studies in neuroscience and neural engineering

New Product Test Engineer May 2013 – Dec. 2013

Trane: Nexia Home Controls Division

- Created automated electrical and mechanical test fixtures for intelligent home control systems
- Managed field trials of over 15 candidates for new home control system prior to product launch
- Worked with international teams from China and India on computation fluid dynamics simulations and firmware development
- Reported new product test findings in detailed presentation at internal design review board that included Trane's chief engineer
- Debugged hardware and firmware of Nexia home automation devices

Related Skills & Coursework:

Programming and Physical Skills

MATLAB; Labview; SimuLink; Mathematica; C++; Eagle PCB; Multisim; SolidWorks; Excel; Sharepoint; Powerpoint; Outlook; Visual Studio; Soldering; Milling; Scroll Saw; Drill Press; Laser Cutting; Water Jet Cutting; 3D printing

Relevant Coursework

Neural Interfaces; Brain-Computer Interfaces; Electromagnetic Fields; Numerical Methods; Artificial Organs; Biomedical Instrumentation; Cell & Molecular Biology; Strength of Materials; Materials Engineering; Thermodynamics; Circuit Design

Awards & Achievements:

Academic Excellence Scholarship Aug 2010 – Aug 2014

- Semester-by-semester scholarship awarded for remaining in good GPA and activity standing with the Schreyer Honors College

Penn State College of Engineering Research Initiative Grant June 2014 – Aug. 2014

- Characterized temperature performance of thin, through-film Vanadium Oxide thermistors on flexible polyimide substrate
- Interfaced arrays of temperature sensors with acquisition electronics for purpose of characterizing seizure activity in brain

Fair Wages for Workers with Disabilities Act (H.R. 831) Feb. 2013

- Helped edit language of and gain congressional endorsement for passing national legislation supporting equal worker rights

2010 West Point Bridge Design National Champion May 2010

- Designed most economical virtual bridges in three-round nationwide competition using West Point Bridge Designer software

Clubs & Activities

Financial Trading Sept 2013 - Present

- Perform technical analysis on securities charts in stock and crypto-currency markets to grow personal trading accounts

Member: Penn State Boxing Team June 2014 - Present

Member: Penn State Chess Club Jan. 2013 - Present

Treasurer: Penn State Undergraduate Association of Blind Students Sept 2012 – May 2013